Revalidation of *Manis aurita*, based on integrative morphological and genomic evidence

Narayan Prasad Koju[1,2,3,4]#, Zeling Zeng[1]#, Guihua Zhang[1]#, Xia Huang[1]#, Zhicheng Yao[1], Xiaoyun Wang[1], Melissa T.R. Hawkins[5], Arlo Hinckley[5,6], Mary Faith C. Flores[5], Ce Guo[7], Jun Li[7], Devendra Maharjan[8], Lianghua Huang[9], Wenhua Yu[1], Liang Leng[10], Kai He[1*], Anderson Feijó [11,*], Yan Hua[7]*

#: equal contribution

*: corresponding authors

Address:

[1] Key Laboratory of Conservation and Application in Biodiversity of South China, School of Life Sciences, Guangzhou University, Guangzhou 510006, China

[2] Center for Postgraduate Studies, Nepal Engineering College, Pokhara University, Lalitpur, Nepal

[3] Key Laboratory of Genetic Evolution and Animal Models, Kunming Institute of Zoology, Chinese Academy of Sciences, Kunming, Yunnan 650201, China

[4] Department of Psychology, University of Washington, Seattle, WA 98125, USA

[5] Division of Mammals, Department of Vertebrate Zoology, National Museum of Natural History, Smithsonian Institution, District of Columbia, Washington, USA

[6] Departamento de Zoología, Universidad de Sevilla, Seville, Spain

[7] Guangdong Provincial Key Laboratory of Silviculture, Protection and Utilization, Guangdong Academy of Forestry, Guangzhou, China

[8] Natural History Museum, Tribhuvan University, Nepal

[9] Wildlife Forensic Science Service, Kunming, Yunnan 650201, China

[10] Chengdu University of Traditional Chinese Medicine

[11] Negaunee Integrative Research Center, Field Museum of Natural History, Chicago, IL, 60605, USA

Abstract

Cryptic diversity within Asian pangolins has long complicated taxonomic clarity, deterring conservation efforts for one of the most heavily trafficked mammalian lineages. In this study we provide strong genomic and morphological evidence to validate *Manis aurita* Hodgson, 1836 a historically described but taxonomically neglected pangolin from the Himalayan region as a distinct species. We demonstrate that *M. aurita* forms a genetically distinct clade, diverging from *Manis pentadactyla* sensu stricto approximately 1.2 million years ago during the early Pleistocene through genome resequencing, mitochondrial phylogenetics, and single-copy ortholog analyses. Morphometric analyses, including linear cranial and external measurements as well as 3D geometric morphometrics, consistently differentiate *M. aurita* from *M. pentadactyla*, with significant variation in skull size, nasal morphology, and external traits such as ear size and tail length. Population genomic analyses reveal that *M. aurita* exhibits reduced recent inbreeding compared to *M. pentadactyla*, yet both species show declining effective population sizes since the Middle Pleistocene. Negligible interspecific gene flow highlights their long-term evolutionary isolation. Genomic islands of divergence are enriched for olfactory receptor genes, suggesting possible ecological adaptation. Therefore, we formally establish *Manis aurita* (common name Himalayan pangolin) as a valid species under the International Code of Zoological Nomenclature, rejecting its former synonymy with *M. pentadactyla* and *M. indoburmanica*. *M. aurita*, endemic to the Himalayan foothills of Nepal, South Tibet and northeastern India, has a narrow distribution and unique evolutionary trajectory, inferring it highly vulnerable to ongoing anthropogenic threats. Our findings have direct implications for forensic traceability, law enforcement, and species-specific conservation planning across Himalaya.

Keywords: cryptic species, genomic divergence, morphometrics, integrative taxonomy, Himalayan pangolin, conservation genetics

Introduction

Pangolins (Order Pholidota) are unique mammals characterized by their keratinized scales, an extraordinary trait among mammals (Challender et al., 2019). These animals face severe threats

including habitat loss and extensive illegal trade, which has resulted in dramatic population declines (Challender et al., 2020b; Zhang et al., 2020; Zhang et al., 2022). Consequently, all pangolin species are listed under Appendix I of the Convention on International Trade in Endangered Species of Wild Fauna and Flora (CITES) and are recognized as Evolutionarily Distinct and Globally Endangered (EDGE) species (Zoological Society of London, 2014). Accurate species identification, clarification of species distribution, and estimation of population sizes and genetic load are essential for effective conservation efforts.

Until recently, eight extant pangolin species were recognized: four in Africa and four in Asia (Gaubert et al., 2018). All Asian species belong to the genus *Manis*, including Chinese pangolin (*M. pentadactyla*), Indian pangolin (*M. crassicaudata*), Sunda pangolin (*M. javanica*), and Philippine pangolin (*M. culionensis*). Recent genomic studies revealed cryptic genetic and taxonomic diversity within Asian pangolins. For instance, genome sequencing of confiscated scales uncovered a cryptic lineage, provisionally named "mysteria", for which no voucher specimens or precise locality data exist (Gu et al., 2023). Moreover, analyses of broad sampling within *M. pentadactyla* have revealed distinct clades, indicating the existence of an undescribed species.

The Chinese pangolin is distributed across a broad range, extending from Nepal in the west to the eastern coast of China, with insular populations on Hainan and Taiwan islands. Latitudinally, its range extends from central China southward to Southeast Asia (Challender et al., 2020a). This broad distribution is divided by geographic barriers, such as the mountains of southwestern China and southward-flowing river systems, which likely drive genetic divergence among geographic populations (He & Jiang, 2014; Koju et al., 2017). Accordingly, Hu et al. (2020a) identified two major clades within *M. pentadactyla*, namely, MPA and MPB. While recent studies have found additional subclades closely related to MPA in China and Southeast Asia (Wang et al., 2022; Wei et al., 2024), MPB remains the most genetically divergent lineage, and its geographic origin has been enigmatic. Initially, the MPB clade was known almost exclusively from specimens confiscated along the Sino-Myanmar border, suggesting a Myanmar origin. This inference was tentative, as the area is a major wildlife trafficking hub (Nijman et al., 2016; Zhang et al., 2017; Bashyal et al., 2021; Gomez et al., 2023; Koju & Tamang, 2025). However, recent studies found occurrences of MPB in Nepal and South Tibet (Koju, 2018; Shrestha et al., 2020; Hogan et al., 2025; Wangmo et al., 2025).

Historically, three subspecies of *M. pentadactyla* were recognized: the nominate subspecies *M. p. pentadactyla* Linnaeus, 1758 described based on specimens from Taiwan (Corbet & Hill, 1992); *M. p. pusilla* Allen, 1906 from the Hainan Island; and *M. p. aurita* Hodgson, 1836 from the central Nepal (Wilson & Mittermeier, 2018). While the former two have been subject to extensive genetic studies (Gaudin et al., 2009; Hu et al., 2020a; Wang et al., 2022; Heighton et al., 2023; Wei et al., 2024), and their evolutionary relationships as well as distribution in China and SE Asia has been confirmed (Hu et al., 2020a; Wei et al., 2024), the taxonomy and evolutionary history of *M. p. aurita* remains unclear.

Recently, Wangmo et al. (2025) describe a new species, *Manis indoburmanica*, from South Tibet, which highlights several challenges in modern taxonomy. The recognition of this new species is based solely on the mitochondrial genome, a data source susceptible to introgression, incomplete lineage sorting, and maternal inheritance bias (Funk & Omland, 2003; Ballard & Whitlock, 2004; Toews & Brelsford, 2012). Furthermore, the work lacks a comprehensive morphological comparison with *M. pentadactyla*, thus failing to establish a clear morphological boundary for *M. indoburmanica*. Critically, as noted by Zijlstra (2025), the authors did not evaluate whether their samples correspond to existing historical names like *M. p. aurita* (Hodgson, 1836) or *M. assamensis* (Fitzinger, 1872), leaving the novelty of the taxon in question. Such challenges underscore the necessity of integrative taxonomic approaches that incorporate genome-wide data, robust morphological comparisons with both *M. pentadactyla* and *M. p. aurita* (Padial et al., 2010; Schlick-Steiner et al., 2010; Fujita et al., 2012).

To resolve this taxonomic uncertainty, we employed an integrative taxonomic framework combining genomic and morphological evidence. Our genomic analyses incorporated topotypical specimens of *M. p. aurita*, while our morphological comparisons included an examination of the external characteristics of its type specimen. The objective of this study was to evaluate whether pangolins from South Asia correspond to the subspecies *aurita* and, if so, whether their degree of divergence supports elevation to full species status. Our analyses reveal clear and pronounced differentiation from *M. pentadactyla* across both genetic and morphological datasets, providing robust support for recognizing this lineage as the distinct species *Manis aurita* Hodgson, 1836.

Result

Phylogenetic relationships and distribution of *Manis pentadactyla*

We firstly estimated the Asian pangolins' phylogeny using 68 mitogenomes (**Table** S1). The maximum likelihood (ML) tree is well-resolved, with every interspecific relationship strongly supported (i.e., bootstrap support [BS] = 100; **Fig**. 1A). The topology aligns well with previous studies (Hu et al., 2020a; Wang et al., 2022; Gu et al., 2023; Wei et al., 2024; Wangmo et al., 2025), reaffirming *Manis pentadactyla* sensu lato (including all three subspecies *pentadactyla*, *pusilla*, and *aurita*) as the sister clade to all other Asian congeners. The putative taxon "mysteria" emerges as the immediate sister to *M. javanica*. *M. pentadactyla* s. l., is represented by 43 samples, clustered into two deeply diverged clades, corresponding to MPA and MPB identified in Hu et al. (2020a).

We further estimated maximum-likelihood trees using autosomal and sex-chromosome derived SNP and single-copy orthologues for a subset of samples (**Table** S2). The phylogenies derived from all three datasets are topologically identical (**Fig**. 1A, **Fig**. S1, S2), mirroring the mitochondrial phylogeny. When projected the SNP of *Manis* species onto principal-component space, every *M. pentadactyla* s. l. sample falls into a tight cluster that is clearly distinct from the other congeneric species (**Fig.** 1B, **Fig**. 1C). Restricting the analysis to *M. pentadactyla* s. l. reveals non-overlapping splitting between MPA and MPB along PC1 (Tracy-Widom test, $p = 1.09 \times 10^{-5}$; **Table** S3), underscoring consistent genomic differentiation despite their close relationship. The result of ADMIXTURE analysis echoes these patterns (**Fig**. 1D). The lowest cross-validation error occurs at K = 2 (CV = 0.50), with marginal increases at K = 3 and K = 4 (CV = 0.53 in both cases; **Table** S4). At K = 2, the inferred clusters correspond closely to MPA and MPB, with three individuals displaying minor ancestry from the opposite cluster. Taken together, the concordant mitochondrial and nuclear results support a robust validation of the split within *M. pentadactyla* sensu lato.

To define the geographic distribution of the MPB clade, we augmented our dataset with publicly available mitochondrial *CYTB* and *COI* sequences from *M. pentadactyla* s.l. A phylogenetic analysis of this expanded dataset confirmed the same backbone topology as our initial trees (**Fig. 2A**). Critically, this analysis placed sequences from specimens described as *Manis indoburmanica* (from South Tibet) firmly within the MPB clade. Furthermore, every MPB haplotype with a reliable geographic origin was traced to either Nepal, South Tibet or Assam,

India a region that includes the collection locality of Hodgson's *aurita* topotype from central Nepal (**Fig.** 2B). This direct association of the MPB clade with the *aurita* topotype provides evidence to assign this lineage, geographically rooted in Nepal, South Tibet and Northeastern India, to *M. aurita*.

Morphometric evidence for the distinctiveness of *M. aurita*

To assess whether *M. aurita* is morphologically distinct from the *M. pentadactyla* sensu stricto (including subspecies *pentadactyla* and *pusilla*) and thus merits recognition as a separate species, we employed linear measurements-based and three-dimensional landmark-based geometric morphometric analyses (**Table** S5). Principal Component Analysis (PCA) of 20 cranial measurements for 44 specimens positioned *M. pentadactyla* s. l. within a morphospace that showed partial overlap with the Indian pangolin (*M. crassicaudata*) but remained clearly separated from the Sunda (*M. javanica*) and Philippine (*M. culionensis*) pangolins (**Fig**. 3A; **Fig.** S3; **Fig**. S4A, S4B). Along PC1, which accounted for 39.4% of the shape variance and primarily reflected overall cranial size, specimens identified as *M. aurita* consistently occupied the positive extreme. This placement indicates that *M. aurita* possesses a significantly larger skull, and proportionally shorter palatine when compared to *M. pentadactyla* s.s. (**Table** S6A-6C).

Three-dimensional landmark-based geometric morphometric analyses of 75 cranial landmarks (**Table** S6) obtained from micro-CT scans also clearly distinguished *M. aurita* from *M. pentadactyla* s.s. along PC3 (**Fig**. 3B, **Table** S8A-8B), but not PC1 or PC2 (**Fig**. S4C, S4D). Compared to *M. pentadactyla* s.s., *M. aurita* exhibits a relatively shorter yet broader nasal bone, a laterally expanded junction between the maxilla and palatine bones, a posteriorly positioned anterior point of the foramen magnum on the ventral occipital surface (landmark 25, see **Table** S6; **Fig.** S5), and an anteriorly shifted M-shaped suture between the maxilla and palatine bones in ventral view, culminating in a shorter ventral maxilla (**Fig.** S10C).

To further substantiate the morphological separation between *M. aurita* and *M. pentadactyla* s.s., we conducted a PCA based on fourteen external body measurements including *M. aurita* and *M. pentadactyla* s.s. and *M. javanica*. A crucial aspect of this analysis was the inclusion of the *M. aurita* holotype (Natural History Museum, BMNH: 43.1.12.85), which notably lacks skull material. The results demonstrated a clear distinction: all specimens from South Tibet, Northeastern India and Nepal, including the *M. aurita* holotype, separated unequivocally from *M. pentadactyla* s.s. along both PC1 (accounting for 52.1% of variance) and PC3 (6.9% of

variance) (**Fig**.3C; **Table** S9A-9C, **Fig**. S4E， S4F). The PCA-based separation is strongly supported by *t*-tests on individual cranial (**Fig**. 3D, **Fig**. S6A; **Table** S10) and external measurements (**Fig**. 3E， **Fig**. S6B, **Table** S11), which show *M. aurita* having significantly longer body lengths, tail lengths, larger hind feet, an extended snout and markedly smaller ears.

Finally, Canonical Variate Analyses (CVA) that using both cranial and external variables achieved 100% classification accuracy in separating *M. aurita* and *M. pentadactyla* s.s. (**Table** S12, S13, 14; **Fig.** S7). In contrast to these clear differences in skeletal and external body proportions, an analysis of scale characteristics using superimposed, scale-encoded heatmaps of 12 intact body skins (nine *M. pentadactyla* s. s. and *three M. aurita*) revealed no significant differences in either the total number of scale rows or their spatial distribution between the two taxa (**Fig**. S8; **Table** S15). Collectively, the consistent and pronounced size- and shape-based differences in both cranial and external morphology, strongly demonstrate that *M. aurita* is morphologically distinct from *M. pentadactyla* s.s. supporting its full species status.

Evolutionary and demographic history of *Manis aurita*

We estimated divergence time of pangolins using 200 selected clock-like single-copy orthologous genes. The most recent common ancestor (MRCA) of the genus *Manis* was dated to approximately 20.1 million years ago (Ma) (95% confidence interval [CI] = 17.5 to 22.6 Ma; **Fig. 4A**), a finding consistent with Gu et al. (2023). *M. aurita* (MA hereafter) and *M. pentadactyla* s. s. (MP hereafter) diverged approximately 1.2 Ma (95% CI = 0.9 to 1.7 Ma), during the early Pleistocene. Pairwise Sequentially Markovian Coalescent (PSMC) analyses revealed MP maintained a larger effective population size (N□) than MA following their divergence (**Fig.** 4B). After their split, the trajectory for MP was characterized by an initial decline, a subsequent period of prolonged stabilization since 1.0 Ma and a final, sudden drop around 50 ka. The trajectory for MA was broadly similar, showing stability until approximately 300 ka, at which point it entered a sustained decline.

As both species experienced population declines and possess small effective population sizes (N_e), we evaluated whether population decline resulted from inbreeding. The histogram of ROH length (**Fig.** 4C) shows that individuals of MP carry more medium- and long-tract ROHs (>100 kb) than those of MA, indicating a higher degree of recent inbreeding. Consistent with this, the median F_{ROH} in MP is ~0.0447, twice that of MA (~0.0228) (**Fig.** 4D). This finding confirms that

MP has undergone more recent inbreeding which may be related to the abrupt Ne drop in the recent past. It is also noteworthy that some individuals in both species exhibit very high FROH (> 0.1), suggesting pronounced inbreeding in certain populations such as *M aurita* near Kathmandu Valley (e.g., Dhading).

We subsequently investigated patterns of interspecific gene flow involving MA to assess the impact of current and historical range overlap with its congeners (**Fig.** 2B). D-suite analyses indicated significant, albeit low-level, introgression from the Indian pangolin (*M. crassicaudata*) into both MP (f4-ratio ≈ 0.0025, p < 1x10-15) and MA (f4-ratio ≈ 0.0022, p < 1x10-15) (**Fig.** 4E; **Table** S16). Evidence of introgression from MA into the Malayan pangolin (*M. javanica*) was also detected by Dsuite (f4-ratio ≈ 0.0017) and TreeMix (**Fig.** 4F). In contrast, when we specifically examined gene flow between MP and MA post-divergence using fastsimcoal2, the analysis strongly favored a scenario of no gene flow over alternative models (ΔAIC > 2.9; **Table** S17). Collectively, these results indicate that while MA has experienced minimal introgression from other pangolin species, it has remained largely isolated from its sister species MP since their divergence.

Finally, we compared MA and MP genomes for signatures of local adaptation by calculating nucleotide diversity (π) and fixation index (F_{ST}), and absolute genetic differentiation (D_{XY}) (**Fig.** S9). Genomic islands of divergence were defined as windows in the top 5 % for both F_{ST} (>0.8575) and D_{XY} (>0.0373; **Fig.** 4G). Gene Ontology (GO) enrichment analysis of genes within these identified islands revealed significant enrichment for terms related to olfactory functions, notably “detection of chemical stimulus involved in sensory perception of smell” and “sensory perception of smell.” (**Fig.** 4H).

Discussion

The Revalidation of *M. aurita*

Despite accumulating molecular evidence suggesting overlooked, or cryptic species (Hu et al., 2020a; Wang et al., 2022; Wei et al., 2024), the taxonomy of *M. pentadactyla* s. l. lacked rigorous examination. Our mitochondrial and genome-wide phylogenomic analyses consistently reveal a divergence between *aurita* and *M. pentadactyla* s.s. (including *M. p. pentadactyla* and *M. p. pusilla*) at about 1.3 Ma (**Fig.** 4A). The magnitude of this split surpasses commonly accepted thresholds for intraspecific variation (Rieseberg & Burke, 2001; Abreu et al., 2025; Van Elst et

al., 2025). Complementing this genetic divergence, morphometric analyses identify consistent and diagnostic differences that distinguish *aurita* from *M. pentadactyla* s.s. (**Fig.** 3). Cranially, *M. aurita* possesses a significantly larger overall skull with a proportionally shorter and broader nasal region compared to *M. pentadactyla* s.s. (**Fig.** S10, S11, **Table** S9, **Table** S10). External morphological differences are particularly clear and facilitate differentiation. For instance, *aurita* has obviously smaller ears than *M. pentadactyla*, a characteristic reflected in its original specific epithet (*aurita*, Latin for eared). On the other hand, our phylogenetic analysis fails to resolve *M. p. pentadactyla* and *M. p. pusilla* as two distinct evolutionary entities (Fig. 1A).

The distribution of *M. aurita* is associated with the Himalayan region (Fig. 2B) encompassing Nepal, South Tibet and northeastern India. It includes the type locality of *M. aurita* from central Nepal, as well as individuals from South Tibet recently described as *Manis indoburmanica* (Wangmo et al., 2025). In contrast, *M. pentadactyla* s.s. is predominantly found in South and Eastern China and Southeast Asia. This geographical separation is likely influenced by biogeographic barriers, such as the rivers run in north-south directions (e.g., the Brahmaputra River) (Lehman et al., 2006; Hu et al., 2020b) and the Arakan Mountains (Hinckley et al., 2024).

Collectively, the congruent evidence from our genetic, morphological, and distributional analyses unequivocally supports recognizing Hodgson's *aurita* as a distinct species. While Zijlstra (2025) previously argued for its revalidation, our study substantiates this view with broader and more integrative evidence. Consequently, in accordance with the Principle of Priority of the International Code of Zoological Nomenclature (ICZN), we reinstate *Manis aurita* Hodgson, 1836 as the valid name for this species. This action renders junior synonyms such as *Pholidotus assamensis* Fitzinger, 1872, and *Manis indoburmanica* Wangmo, Ghosh, Dolker, Joshi, Sharma and Thakur, 2025.

Evolutionary history of *M. aurita*

The population genetic and demographic analyses illuminate the evolutionary trajectory of *M. aurita* following its speciation. The ancestors of *M. aurita* and *M. pentadactyla* diverged in the early Pleistocene, period of, significant global climatic oscillations. Given that pangolins are generally warm-adapted species, with no historical fossil evidence suggesting their presence in northern China (Tong, 2007), the climatic shifts likely played a crucial role in driving the allopatric separation of the ancestor into western (Himalaya) vs. eastern (East/ South East Asia) refugium (Louys & Meijaard, 2010; Leonard et al., 2015; Hawkins et al., 2016; Camacho-

Sanchez et al., 2017; Hinckley et al., 2023). Pangolins are highly olfactory-reliant mammals, exhibiting significantly enlarged olfactory bulb (Imam et al., 2018; Li et al., 2024), using smell to forage for ants and termites (DiPaola et al., 2020). As the *M. aurita* and *M. pentadactyla* adapted to their respective environments, certain OR genes, certain OR genes likely diverged under selection as supported in our GO enrichment analysis (Fig. 4H).

The population of *M. aurita* decline started around 300 Ka and is consistent with the Penultimate Glaciation (~300–130 Ka), during which the climate cooled and dried (Colleoni et al., 2016; Ma et al., 2022), likely leading pangolin habitats to contract. Notably, similar patterns are seen in other warm-adapted mammals in southern China (Li et al., 2025), such as the golden snub-nosed monkeys (Dai et al., 2024).

Our analyses further detected limited gene flow between *M. aurita* and two other Asian pangolins. The signal of introgression between *M. aurita* and *M. crassicaudata* (contributing to <0.25% of the genome) is unsurprising, given their sympatric ranges in southern Nepal and northeastern India. We also observed a similarly low level of gene flow between *M. aurita* and *M. javanica*, indicating that their distributions likely have overlapped at least historically. Despite these instances of historical admixture, the low level of gene flow indicates *M. aurita* has maintained its status as a distinct evolutionary entity.

It is noteworthy, in the admixture analysis, at both K=3 and K=4, *M. aurita* separated into two distinct genetic clusters: one comprising individuals from Nepal and the other comprising individuals from South Tiber and northeastern India, a pattern that indicates significant intraspecific subdivision.

Conservation Implications

The formal recognition of *M. aurita* as a distinct species carries profound conservation significance. Its intrinsic vulnerability is underscored by a geographically restricted range, confined to the Himalayan–Indo-Burmese region, and a demographic history marked by a more pronounced and sustained population decline since the Middle Pleistocene compared to *M. pentadactyla*.

Despite the long-term population decline revealed by PSMC analyses, *M. aurita* on average exhibits lower levels of recent inbreeding than *M. pentadactyla* as evidenced by the results of ROH and FROH (**Fig.** 4C, D). This likely reflects differing histories of anthropogenic pressure

nowadays; the less intensively developed landscapes of South Asia historically provided more contiguous refuge habitats compared to the range of *M. pentadactyla* in China and Southeast Asia, where has experienced intense human activity for centuries, leading to severe habitat fragmentation and the regional extinction of many medium-to-large mammal species (Brook et al., 2014; Goossens et al., 2016; Boonratana, 2020). However, it is noteworthy, *M. aurita* around Kathmandu valley exhibit extremely high inbreeding levels (i.e., FROH > 0.1), indicating that these populations are already facing severe inbreeding depression (**Fig.** 4D). Conservation strategies must therefore prioritize the identification and management of these highly vulnerable populations to prevent local extinctions.

Overarching these intrinsic vulnerabilities is the critical threat from illegal wildlife trade. Genetic analyses of confiscated scales have repeatedly confirmed that *M. aurita* is a target (Hu et al., 2020a). Alarmingly, our findings also reveal that products from this species have infiltrated regulated traditional medicine markets (data from Xie et al. (2021); **Fig.** S13), demonstrating that illegally sourced materials are being laundered through formal supply chains. The comprehensive genomic dataset presented here, with its improved geographic coverage and inclusion of previously unsampled populations, provides an enhanced genetic baseline which will bolster wildlife forensics by allowing for greater precision in determining the geographic provenance of confiscated scales, thereby helping to pinpoint poaching hotspots.

Taxonomy

Manis aurita Hodgson, 1836 stat. nov.

Manis auritus Hodgson, 1836. Original description.

Manis aurita Waterhouse,1838

Phatages bengalensis Fitzinger, 1872

Pholidotus assamensis Fitzinger, 1872

Manis pentadactyla auritus Thomas 1918

Manis pentadactyla Ellerman & Morrison-Scott, 1951 (part)

Manis indoburmanica Wangmo, Ghosh, Dolker, Joshi, Sharma and Thakur, 2025

Holotype: BMNH 43.1.12.85, an adult (skin) collected by Brian Houghton Hodgson in 1836 from Central Nepal (**Fig.** S11B).

Emended diagnosis: *Manis aurita* can be diagnosed by the following combination of characters that distinguish it from all other Asian pangolins: the external pinna is small and distinctively flake-shaped. On the snout, the first row of head scales lies well behind the nasal tip, exposing a bare patch of naked skin (**Fig**. S10A); dorsal scales are smooth and trapezoidal with straight posterior margins, whereas the lateral scales near the abdomen are broad and shield-shaped (**Fig**. S10B). Cranially, the palatal process of the premaxilla extends posteriorly but measures less than half of the premaxillary midline length, and the incisive foramen does not extend to the premaxilla's posterior border. At its anterior end, the maxilla bulges laterally, creating nearly parallel lateral margins (**Fig**. S10C). The postglenoid foramen opens laterally within the central region of the postglenoid fossa. (**Fig**. S10D). Both the jugular and hypoglossal foramina are recessed yet remain distinct. Finally, the ventral surface of the occipital condyle is flat rather than convex (**Fig**. S10C).

Description: *Manis aurita* is an Asian pangolin with an elongated head, small ears, short limbs, and a tail shorter than half the body length. Its external pinna is small and flake-shaped. The head and body are covered in overlapping, exceptionally smooth keratin scales: dorsal scales are trapezoidal with straight posterior edges, while lateral abdominal scales are broad and shield-shaped. On the snout, the first row of head scales lies well behind the nasal tip, leaving a bare patch of skin. The ventral surface is pale brown and densely fringed with short, stiff hair bristles. Claws are moderately curved: the third (middle) claw on each forefoot is the longest, the first and fifth claws are noticeably shorter, and all hind-foot claws are shorter than those on the forefeet. Scale coloration in adults ranges from dark brown to chestnut; juveniles are slate-grey or grey-brown, with more bristles between scales.

The skull exhibits a relatively elevated and broad profile. The ventral palatal process of the premaxilla is short, measuring less than half the length of the premaxilla itself. The incisive foramen of the premaxilla does not contact the ventral projection of the maxilla. The vomer does not protrude at the midline on the ventral surface of the maxilla. The nasal bones are broad and terminate in a semicircular shape. The postglenoid foramen is positioned laterally. The pterygoid hamulus is short and does not extend beyond the ectotympanic bulla, which is rounded in shape. The palatine sutures form an M-shaped structure. The zygomatic process of the maxilla may either be connected to the zygomatic process of the squamosal via a bony rod-like structure or

remain unconnected. The external and skull measurements are presented in Supplementary Data 1,2, respectively.

The total number of body scales ranges from 538 to 596. From the neck to the tail base there are 254–274 scales arranged in 23–24 longitudinal and 15–17 transverse rows. The tail bears 140–153 scales: 80–94 on the dorsal surface organized into five transverse by 16–20 longitudinal rows, and 50–63 on the ventral surface in three to five transverse by 18–20 longitudinal rows, with 17–19 scales along each lateral edge. The forelimbs carry 37–55 scales per side, while the hindlimbs have 32–41 scales per side.

Comparisons

Manis aurita (MA) and *M. pentadactyla* s.s. (MP) share a close morphological resemblance, exhibiting a similar number of body scales, typically uniform dark brown to deep chestnut. These scales are generally shield-shaped or trapezoidal and are interspersed with sparse hair bristles (**Fig.** S11A). This contrasts with *M. javanica*, whose scales on the tail tip, tail base, and ventral side are pale yellow, and which uniquely features a reversed growth direction in the last longitudinal scale row on its forelimbs. *M. crassicaudata* is set apart by its larger, earth-toned scales and the absence of interspersing hair bristles. *M. culionensis* is characterized by more numerous, elongated, and sharper-tipped scales that are dark brown and either leaf-shaped or shield-shaped. In MA and MP, the zygomatic process of the maxilla and the squamosal is sometimes connected via a bony rod to form a zygomatic arch. This contrasts with all other species, that lack a complete zygomatic arch. The palatal process of the premaxilla in MA and MP is notably short, not exceeding half the premaxilla's midline length, unlike in other species, where this process is longer (**Fig.** S11B). Additionally, the postglenoid foramen in MA and MP opens on the lateral aspect of the zygomatic process, differing from *M. javanica* and *M. culionensis*, where it opens posteriorly, and from *M. crassicaudata*, where its opening can be either posterior or lateral (**Fig.** S11B).

Compared to MP, MA typically attains a larger adult body size, with a total body length ranging from 81.0 to 105.1 cm (mean: 95.2 cm) compared to 60.5 to 80.6 cm in MP (mean: 71.2 cm). MA also possesses a longer tail (31.7–40.9 cm, mean: 37.4 cm) than MP (22.3–31.6 cm, mean: 27.5 cm), and has larger foot surfaces, with hindfoot lengths averaging 6.4 cm versus 2.9 cm in MP. Furthermore, the external pinnae differ, with those of MA being distinctly smaller than in MP (Fig. 3E; Fig. S6B). The skull of MA is larger and taller than that of MP, with cranial width

ranging from 93.2 to 99.7 mm (mean: 95.6 mm) and height from 35.2 to 36.3 mm (mean: 35.8 mm), compared to MP's cranial width of 75.9 to 95.9 mm (mean: 84.6 mm) and height of 23.8 to 31.5 mm (mean: 27.6 mm). Additionally, the maximum width of the gap between the maxillary bones is wider in MA (13.5–14.7 mm, mean: 13.8 mm) than in MP (10.1–12.0 mm, mean: 10.9 mm).The skull of MA is larger and taller than that of MP. This is reflected in a relatively smaller nasal length-to-width ratio in MA (approximately 1.9:1), indicating a broader nasal bone, whereas MP has a narrower nasal bone with a larger ratio (approximately 2.5:1), resulting in a comparatively more slender nasal region (**Fig.** 3D; **Fig.** S6A). The anterior portion of the skull in MA is also broader and deeper; its maxillary region expands laterally, with the posterior lateral margins of this anterior expansion running nearly parallel. In contrast, the anterior part of the skull in MP is more elongated, contributing to a more triangular overall shape of the ventral skull surface. The palatine bone in MA is positioned more anteriorly than in MP. Specifically, the most posterior point of the palatine sutures in MA aligns approximately with the maxilla zygomatic process and squamosal zygomatic process junction. In MP, however, this point lies posterior to this junction. The occipital condyle also shows clear differences: in MP, it is distinctly prominent, whereas MA presents a relatively flat ventral condylar articular surface that extends posteriorly. The condylar articular facet is comparatively smaller in MP than in MA (**Fig.** S11A).

Distribution, habitat, and Conservation Statues

Manis aurita is distributed along the southern Himalayan foothills, with confirmed occurrences in Nepal, South Tibet and northeastern India (including Assam), southern Bhutan, and extending into southern Tibet. The species' altitudinal range spans from lowland areas to approximately 3,000 meters above sea level. The eastern extent of its distribution remains undefined, but the Arakan Mountains appear to represent the eastern geographic limit for this species (Hinckley et al., 2024). Further surveys are necessary to ascertain its potential presence in Myanmar.

Manis aurita predominantly inhabits mixed deciduous and evergreen forests. Key tree species in these habitats include *Shorea robusta*, *Schima wallichii*, *Castanopsis indica*, and *Alnus nepalensis*. *M. aurita* is also frequently observed in forested areas adjacent to human-modified landscapes, indicating some level of adaptability to disturbed environments (Thapa et al., 2014; Dhital et al., 2020; Shrestha et al., 2021).

Despite protected under national laws such as the Nepal's National Parks and Wildlife Conservation Act (1973), India's Wildlife Protection Act (Schedule I, 1972), and internationally under CITES Appendix I, *M. aurita* remains a significant target for illegal wildlife traffickers in South Asia. For example, Kathmandu functions as a major transit hub for smuggled pangolin scales (Bashyal et al., 2021; Koju & Tamang, 2025). Similar trafficking pressures are evident in neighboring India and Bhutan, where challenges such as limited enforcement capacity and porous international borders facilitate cross-border smuggling operations.

Material and Methods

Taxon sampling and sequencing

DNA was extracted from tissue samples (n=18) and purified using the Dneasy blood and tissue kit (Qiagen). Genomic DNA was sheared to ~350 bp fragments using a Covaris LE220R-plus system (Covaris, USA), followed by end-repair, A-tailing, and adapter ligation. Libraries were amplified by PCR, purified with AMPure XP beads.

Destructive sampling was conducted using skin specimens deposited in the National Museum of Natural History, the Smithsonian Institution (USNM), Field Museum of Natural History (FMNH); American Museum of Natural History (AMNH) and University of Michigan, Museum of Zoology (UMMZ) in the United States. Sterile practices were employed with routine bleaching, instrument sterilization, and changing of PPE to prevent any cross contamination between specimens. Samples of 25 mg of material were placed in sterile cryovials or 1.5mL tubes and transferred to a dedicated Historic DNA processing facility at the Smithsonian Institution's Museum Support Center where DNA extraction was performed via Qiagen MinElute or Investigator kits following the manufacturer's protocol. Single-stranded library preparation was performed with the SRSLY Pico Plus Kit (Claret Biosystems®) utilizing half reactions. Libraries had dual indexed iTru style adapters ligated to each sample and amplified for 18 cycles of PCR. Following amplification, samples were visualized on a High-Sensitivity Tape Station (Agilent), and pooled in equimolar ratios for sequencing.

Sequencing was performed on an Illumina NovaSeq X platform to generate 150 bp paired-end (PE150) reads. Raw FASTQ reads were processed with fastp v0.24.0 (Danecek et al., 2021) to remove adapter contamination and poly-G tails, trimming bases with Phred score ≤ 5. Reads containing > 10 % ambiguous bases or > 50 % low-quality bases were discarded. We supplemented our dataset with 48 available genome re-sequencing data including 24 *M.*

pentadactyla, 19 *M. javanica*, 2 *M. crassicaudata*, 1 *Phataginus tricuspis*, and 1 *Smutsia gigantea* (**Table** S5).

Mitochondrial assembly and phylogenetic analyses

Mitochondrial genomes were assembled from 64 raw sequencing datasets, including data from 30 newly sequenced individuals and 34 previously published genomes of various pangolin species. For these datasets, clean reads were processed for *de novo* assembly and annotation in MITOZ v3.6 (Meng et al., 2019), which employed Megahit with k-mer values of 21, 33, and 55. This final set of assembled mitogenomes was then augmented with five additional mitogenomes obtained from GenBank (**Table** S1). We aligned mitogenomes using MAFFT v7.5 (Katoh & Standley, 2013), and trimmed poorly aligned regions using Gblocks. We retained 12S, 16S rRNA, and 12 coding genes on the heavy chain for phylogenetic analyses. We also downloaded available mitochondrial 18 *CYTB* and 12 *COI* genes identified as *M. pentadactyla* from GenBank. We used IQ-TREE v2.1.3 to estimate the best-scoring Maximum-likelihood (ML) trees. ModelFinder was used to automatically determine the optimal partitioning scheme and substitution models under the Bayesian Information Criterion (–m MFP+MERGE). Node support was evaluated with 1,000 ultrafast bootstrap replicates.

Genome assembly and phylogenetic analyses

We aligned clean data to a *M. pentadactyla* reference genome (GCF_030020395.1) using BWA v0.7.17. The resulting SAM files were converted to coordinate-sorted BAMs and indexed with SAMtools v1.10 (Li et al., 2009). Duplicates were identified and flagged using MarkDuplicates tool of GATK v.4.6 (McKenna et al., 2010). Local realignment around indels was then performed using GATK's IndelRealigner to reduce false-positive variant calls. Per-sample gVCFs were generated with GATK's HaplotypeCaller and merged via CombineGVCFs. SNP calling was then executed with GenotypeGVCFs and SelectVariants to produce multisample VCF and isolate high-confidence SNP calls, respectively. We filtered SNP calls using GATK's VariantFiltration module with thresholds: QUAL < 30.0, QD < 2.0, MQ < 40.0, FS > 60.0, SOR > 3.0, MQRankSum < –12.5, ReadPosRankSum < –8.0, and SB ≥ –1.0. We applied VCFtools v0.1.16 to remove SNPs with minor-allele frequency < 2 % or depth outside the 2.5–97.5 percentile of the depth distribution (Danecek et al., 2011).

Phylogenetic relationships were inferred using three datasets: high-quality single nucleotide polymorphisms (SNPs) for autosomal and sex chromosomes as well as single-copy

orthologous genes. For the SNP-based analyses, autosomal and sex chromosome SNP data were separately extracted from the filtered, high-quality multi-sample VCF. These datasets were converted to PHYLIP format using vcf2phylip v2.8. ML trees were constructed for both datasets using IQ-TREE v2.1.4 as mentioned above. For the ortholog-based analysis, we first identified 23,752 single-copy orthologs using OrthoFinder v2.5.4 (Emms & Kelly, 2015). These orthologs underwent stringent filtering based on GC content, sequence variability, proportion of missing data, and ambiguous bases, resulting in 7,852 high-quality loci. Each loci was individually aligned and a concatenated ML tree was constructed using IQ-TREE as mentioned above.

Genetic structuring analyses

To investigate population genetic structure, we utilized linkage-disequilibrium (LD)–pruned autosomal SNPs. LD pruning was performed in PLINK v1.90b6.21 using the –indep-pairwise 50 5 0.2 parameters (Purcell et al., 2007). We then performed PCA on mean-imputed genotypes in PLINK to extract the top ten principal components. To assess the statistical significance of the principal components, we applied the Tracy-Widom test implemented in EIGENSOFT v8.0.0 (Patterson et al., 2006). We applied PCA to all *Manis* samples and *M. pentadactyla* sensu lato (which encompasses individuals later identified as *M. aurita*). To infer individual ancestry proportions, we ran ADMIXTURE v1.3.0 on the *M. pentadactyla* s.l. samples. We evaluated models for K (number of ancestral populations) from 1 to 10, and selected the optimal K to minimize cross-validation error (Alexander et al., 2009).

Molecular dating and population genetic analyses

Divergence times were estimated using *BEAST3 model(Douglas et al., 2022) as implemented in BEAST v2.7.7 (Bouckaert et al., 2019). First, we identified the 2,000 most genetically divergent loci from an initial pool of 7,852 filtered orthologs. These loci were then assessed for their conformity to a strict molecular clock using SortaDate v2.0 (Smith et al., 2018). The 200 orthologs that best fit the strict clock model were subsequently used for the divergence time estimation. The Bayesian inference employed a Birth–Death tree prior, a strict molecular clock, and the HKY+Γ substitution model. We employed two secondary calibrations derived from the molecular dating estimates of Gu et al. (2023). The analysis was constrained by setting priors on i) the crown-group pangolin divergence, set to 33.19 million years ago (Ma) (95% CI: 29.8–30.3 Ma), and ii) the divergence of Asian pangolins, set to 16.9 Ma (95% CI: 12.9–22.3 Ma). The Markov chain Monte Carlo (MCMC) analysis was run for 200 million generations. Convergence

and parameter mixing were assessed in Tracer v1.7.2 (Rambaut et al., 2017), ensuring all key parameters achieved effective sample sizes (ESS) > 200.

Historical population dynamics were reconstructed using the Pairwise Sequentially Markovian Coalescent (PSMC) model (Li & Durbin, 2011). According to the estimated divergence time between *M. pentadactyla* and *M. aurita* (see Results), we estimated the mutation rate per generation assuming an average generation time of 7 years (IUCN SSC Pangolin Specialist Group et al., 2018). The analysis was run with the parameters -N25 -t15 -r5 -p "4+25*2+4+6", using the Manis *pentadactyla* genome (Hu et al., 2020a) as the reference for mapping. To assess the variability in demographic inferences, 100 bootstrap replicates were performed.

Levels of inbreeding were quantified by calculating the average inbreeding coefficient (FROH) for each individual. Long runs of homozygosity (ROH) were identified using PLINK v2.0 (Purcell et al., 2007) with the parameters --homozyg --homozyg-window-snp 20 --homozyg-kb 100. Individual FROH values were then calculated as the proportion of the autosomal genome covered by ROH, relative to the total autosomal SNP coverage, following McQuillan et al. (2008).

Geneflow analyses To infer the direction and magnitude of historical gene flow among *Manis* species, we analyzed a high-quality SNP dataset from 52 samples representing the four *Manis* species using Dsuite v0.5 (Malinsky et al., 2021) and TreeMix v1.13 (Pickrell & Pritchard, 2012). We first filtered the SNP dataset to retain sites with ≤20% missing data using VCFtools (--max-missing 0.8). To quantify admixture, we used the Dtrios program in Dsuite to calculate D-statistics and f4-ratio statistics for all relevant population trios. *P. tricuspis* and *S. gigantea* were used as outgroups. Results were visualized with the dtools.py script. To model population splits and migration events, the filtered SNP data was first pruned for linkage disequilibrium (PLINK; --indep-pairwise 50 5 0.6), and the output was converted to TreeMix format using plink2treemix.py. We then ran TreeMix, exploring models with 0 to 5 migration edges (five replicates each). The optimal model was selected by evaluating the explained variance and residual plot fits. The resulting population graph was visualized using the R script plotting_funcs.R provided with TreeMix.

We used FastSimCoal v2.8 (Excoffier et al., 2021) to test potential gene flow between *M. pentadactyla* (MP) and *M. aurita* (MA). First, we used VCF file through easySFS to generated

folded observed joint site frequency spectrum (JSFS). We constructed four demographic models to test gene flow scenarios: (1) early gene flow (range from 120,000 to 130,000 generations); (2) recent gene flow (range from 1,000 to 20,000 generations); (3) continuous gene flow; and (4) no gene flow. For each tested demographic model, we performed 100 independent runs using 100,000 simulations, 40 expectation–maximization cycles, and a broad search range for parameters to determine the run with the best parameter estimates and maximum likelihood. Model comparisons were performed using the Akaike Information Criterion (AIC) to identify the model that best explains the observed data.

Genomic Island of Differentiation

To identify genomic regions under divergent selection, we scanned the genomes of *M. pentadactyla* and *M. aurita*. We used Pixy v2.0 to calculate nucleotide diversity (π), fixation index (F_{ST}), and absolute genetic differentiation (d_{XY}) across 20 kb windows (Korunes & Samuk, 2021). Candidate genomic islands of divergence were defined as outlier windows concurrently in the top 5th percentile for both F_{ST} and d_{XY}. We extracted all genes within these outlier regions. Genes annotated only with LOC identifiers were annotated based on their high-confidence human orthologs, identified via BLASTP (Altschul et al., 1997). This gene set was then tested for Gene Ontology (GO) term enrichment using the R package clusterProfiler (Yu et al., 2012).

Morphometric analyses

We accessed specimens deposited in FMNH, USNM, UMMZ, British Museum of Natural History, UK (BMNH), Natural History Museum, Tribhuvan University (NHM-TU) Institute of Zoology, Guangdong Academy of Sciences, China (IOZ-GDAS), and Guangdong Wildlife Monitoring and Rescue Center, China (GWMRC) (**Table** S5). Fourteen external measurements were taken including full body length (abdominal) (FBLA), head body length (abdominal) (BLA), tail length (abdominal) (TLA), full body length (back) (FBLB), head body length (back) (HBL), tail length (back) (TLB), ear length (EL), ear thickness (ET), middle claw length of the back foot (MCLBF), middle claw length of the forefoot (MCLFF), the distance of the first scale from the tip of the nose (DFSTN), the maximum number of scales in the back of the body (MNS), the single-sided number of tail edge scales (SNTE), length of hind foot (LHF), using soft tape rulers (accurate to 0.1 mm) for flexible dimensions and MNT-150 standard-type zinc alloy digital caliper (Model: MNT952101; DEGUQMNT, accuracy to 0.01 mm) for more precise

linear features (**Fig.** S3A). This data includes 26 skin specimens for *M. pentadactyla* (n=8), *M. javanica* (n=12), *M. aurita* (n=6) and also includes the holotype of *M. aurita*.

Twenty cranial measurements were conducted with MNT-150 standard-type zinc alloy digital caliper (accuracy to 0.01 mm), following (Gaubert & Antunes, 2005; Wu et al., 2005; Gaudin et al., 2009; Sulaiman et al., 2017; Igado et al., 2020; Morenikeji et al., 2022) including total skull length (TSL), nasal to foramen magnum base length (NFBL), premaxilla to palatine (PP), from Intersection between maxilla and palatine sutures to most posterior point of the palatine sutures(IMPS), tymapanic bulla (left) (TB), maximum width between lateral edge of auditory bulla (WSLB), skull height (H), width of Nasal Bone (WN), length of Nasal Bone (LN), dorsal gap between maxillary (dorsal) (GM), maximum width of Gap between maxillary (MWG), left maximal length of orbit left） (MO), distance between auditory bulla (DA), length of suture between parietal bone (DTEM), length of suture between frontal bone (DLOB), zygomatic process between maxilla and squamous bone left） (ZMS), length of foremen magnun occipitals (FMO), mandible length (left) (ML), the distance between condylar process (DCP), length of palatal process of premaxilla(LPP) (Fig. S3B). This data includes 44 skulls for *M. pentadactyla* (n=25), *M. javanica* (n=7), *Manis crassicaudata* (n=2), *M. culionensis* (n=3) and *M. auritus* (n=7). Sex was not considered in the analysis due to the absence of marked sexual dimorphism and the lack of information for some specimens. Specimen age was assessed based on body size, skull morphology, and available collection records. Juvenile and subadult individuals were excluded in the analysis. To ensure completeness of the data, we replaced missing values with the mean value calculated across specimens of the same species. We used the function prcomp () of stat to conduct principal component analysis (PCA) and Morpho to perform canonical variate analysis (CVA) on log□□-transformed variables. Finally, we conducted Levene's test for homogeneity of variances using the leveneTest () function and then performed Student's t-tests with t.test () to compare group means across taxa.

We downloaded 84 micro□CT scan data from Ferreira-Cardoso et al. (2019)**,** and scan 13 specimens, obtaining high□resolution micro□CT scans of 97 skulls for *M. pentadactyla* (n = 42), *M. javanica* (n = 38), *M. crassicaudata* (n = 12), *M. culionensis* (n = 3), and *aurita* (n = 2; **Table** S1). Raw DICOM stacks were imported into Materialise Mimics v19.0 for segmentation and construction of 3D cranial meshes. We placed 75 landmarks per mesh following Ferreira-Cardoso (2020; **Fig.** S5**).** After Procrustes alignment, we conduct principal component analysis

(PCA) and canonical variate analysis (CVA) using MorphoJ v1.08 (Dryden & Mardia, 1993). Landmark selection was based on prior studies addressing mammalian taxa (Goswami, 2006; Hautier et al., 2017)

Scale coding

We generated scale-encoded heatmaps from 12 intact skins (nine *M. pentadactyla*, three *M. aurita*) to visualize variation following Algewatta et al. (2020); Guo et al. (2022) and Martin et al. (2024). In brief, we digitized the x-y coordinates of every scale in Excel, exported standardized images into Photoshop v25, and overlaid all specimens per species to produce species-specific composite maps.

Acknowledgments

We are grateful to the Natural History Museum, Tribhuvan University, and the Department of National Parks and Wildlife Conservation (Nepal) for providing research permissions and institutional support. We sincerely thank the Ministry of Education, Science and Technology, Nepal, and the Nepal Academy of Science and Technology (NAST) for their valuable support during the early stages of this research. We thank the following institutions for providing access to specimens for morphological and genetic analyses: The National Museum of Natural History, Smithsonian Institution (USNM); Field Museum of Natural History (FMNH); American Museum of Natural History (AMNH); University of Michigan Museum of Zoology (UMMZ); Tribhuvan University, Nepal; the Institute of Zoology, Guangdong Academy of Sciences (IOZ-GDAS); and the Guangdong Wildlife Monitoring and Rescue Center (GWMRC), China. Our sincere thanks are also extended to Ms. Saraswoti Byanjankar for her valuable assistance with morphological measurements at the Natural History Museum, UK. This study is supported by the ADCS Seed Grants program of the National Museum of Natural History, Smithsonian Institution (M.T.R.H. and A.H.), Guangdong Provincial Natural Science Foundation for Distinguished Young Scholars (2022B1515020033, K.H.) and the National Natural Science Foundation of China (32170452, K.H.).

References

Abreu, EF, Prado, JR, Maldonado, JE, Wilson, DE, Percequillo, AR, & Pavan, SE. (2025). Recent, Intricate Speciation in Amazonia Uncovered by a Multilayered Genomic

Analysis of Tree Squirrels. Systematic biology, syaf013. https://doi.org/10.1093/sysbio/syaf013

Alexander, DH, Novembre, J, & Lange, K. (2009). Fast model-based estimation of ancestry in unrelated individuals. Genome research, 19(9), 1655-1664. https://doi.org/10.1101/gr.094052.109

Algewatta, HR, Perera, P, Karawita, H, Dayawansa, N, Manawadu, D, & Liyanage, M. (2020). Updates on the morphometric characterization of Indian pangolin (*Manis crassicaudata*) in Sri Lanka. Animals, 11(1), 25. https://doi.org/10.3390/ani11010025

Altschul, SF, Madden, TL, Schäffer, AA, Zhang, J, Zhang, Z, Miller, W, & Lipman, DJ. (1997). Gapped BLAST and PSI-BLAST: a new generation of protein database search programs. Nucleic acids research, 25(17), 3389-3402. https://doi.org/10.1093/nar/25.17.3389

Ballard, JWO, & Whitlock, MC. (2004). The incomplete natural history of mitochondria. Molecular ecology, 13(4), 729-744. https://doi.org/10.1046/j.1365-294X.2003.02063.x

Bashyal, A, Shrestha, N, Dhakal, A, Khanal, SN, & Shrestha, S. (2021). Illegal trade in pangolins in Nepal: Extent and network. Global Ecology and Conservation, 32, e01940.

Boonratana, R. (2020). Asian primates in fragments: Understanding causes and consequences of fragmentation, and predicting primate population viability. American journal of primatology, 82(4), e23082. https://doi.org/10.1002/ajp.23082

Bouckaert, R, Vaughan, TG, Barido-Sottani, J, Duchêne, S, Fourment, M, Gavryushkina, A, Heled, J, Jones, G, Kühnert, D, & De Maio, N. (2019). BEAST 2.5: An advanced software platform for Bayesian evolutionary analysis. PLoS computational biology, 15(4), e1006650. https://doi.org/10.1371/journal.pcbi.1006650

Brook, SM, Dudley, N, Mahood, SP, Polet, G, Williams, AC, Duckworth, J, Van Ngoc, T, & Long, B. (2014). Lessons learned from the loss of a flagship: the extinction of the Javan rhinoceros *Rhinoceros sondaicus annamiticus* from Vietnam. Biological Conservation, 174, 21-29. https://doi.org/10.1016/j.biocon.2014.03.014

Camacho-Sanchez, M, Leonard, JA, Fitriana, Y, Tilak, M-K, & Fabre, P-H. (2017). The generic status of Rattus annandalei (Bonhote, 1903)(Rodentia, Murinae) and its evolutionary implications. Journal of Mammalogy, 98(5), 1340-1355. https://doi.org/10.1093/jmammal/gyx081

Challender, D, Wu, S, Kaspal, P, Khatiwada, A, Ghose, A, Ching-Min Su, N, & Suwal, TL. (2020a). *Manis pentadactyla*. The IUCN Red List of Threatened Species 2019: e.T12764A168392151. In: Gland: IUCN.

Challender, DW, Heinrich, S, Shepherd, CR, & Katsis, LK. (2020b). International trade and trafficking in pangolins, 1900–2019. In Pangolins (pp. 259-276). Elsevier. https://doi.org/10.1016/B978-0-12-815507-3.00016-2

Challender, DW, Nash, HC, & Waterman, C. (2019). *Pangolins: science, society and conservation*. Academic Press.

Colleoni, F, Wekerle, C, Näslund, J-O, Brandefelt, J, & Masina, S. (2016). Constraint on the penultimate glacial maximum Northern Hemisphere ice topography (≈ 140 kyrs BP). Quaternary Science Reviews, 137, 97-112. https://doi.org/10.1016/j.quascirev.2016.01.024

Corbet, GB, & Hill, JE. (1992). *The mammals of the Indomalayan region: a systematic review* (Vol. 488). oxford university press Oxford.

Dai, Y, Xia, W, Zhu, Y, Hacker, C, Wang, X, & Li, D. (2024). Historical changes in the distribution of the Sichuan golden snub‐nosed monkey (*Rhinopithecus roxellana*) in

Sichuan Province, China. Ecology and Evolution, 14(4), e11270. https://doi.org/https://doi.org/10.1002/ece3.11270

Danecek, P, Auton, A, Abecasis, G, Albers, CA, Banks, E, DePristo, MA, Handsaker, RE, Lunter, G, Marth, GT, & Sherry, ST. (2011). The variant call format and VCFtools. bioinformatics, 27(15), 2156-2158. https://doi.org/10.1093/bioinformatics/btr330

Danecek, P, Bonfield, JK, Liddle, J, Marshall, J, Ohan, V, Pollard, MO, Whitwham, A, Keane, T, McCarthy, SA, & Davies, RM. (2021). Twelve years of SAMtools and BCFtools. Gigascience, 10(2), giab008. https://doi.org/10.1093/gigascience/giab008

Dhital, S, Paudel, SM, Thapa, S, Bleisch, WV, Shrestha, A, & Koju, NP. (2020). Distribution of Chinese pangolin (*Manis pentadactyla*) in Nagarjun forest of Shivapuri Nagarjun National Park, Nepal. Nepalese Journal of Zoology, 4(1), 1-7. https://doi.org/10.3126/njz.v4i1.30667

DiPaola, JD, Yindee, M, & Plotnik, JM. (2020). Investigating the use of sensory information to detect and track prey by the Sunda pangolin (*Manis javanica*) with conservation in mind. Scientific reports, 10(1), 9787. https://doi.org/10.1038/s41598-020-65898-x

Douglas, J, Jiménez-Silva, CL, & Bouckaert, R. (2022). StarBeast3: adaptive parallelized Bayesian inference under the multispecies coalescent. Systematic biology, 71(4), 901-916. https://doi.org/10.1093/sysbio/syac010

Dryden, IL, & Mardia, KV. (1993). Multivariate shape analysis. Sankhyā: The Indian Journal of Statistics, Series A, 460-480. https://www.jstor.org/stable/25050954

Emms, DM, & Kelly, S. (2015). OrthoFinder: solving fundamental biases in whole genome comparisons dramatically improves orthogroup inference accuracy. Genome biology, 16, 1-14. https://doi.org/10.1186/s13059-015-0721-2

Excoffier, L, Marchi, N, Marques, DA, Matthey-Doret, R, Gouy, A, & Sousa, VC. (2021). fastsimcoal2: demographic inference under complex evolutionary scenarios. bioinformatics, 37(24), 4882-4885. https://doi.org/10.1093/bioinformatics/btab468

Ferreira-Cardoso, S, Billet, G, Gaubert, P, Delsuc, F, & Hautier, L. (2019). Skull shape variation in extant pangolins (Pholidota: Manidae): allometric patterns and systematic implications. Zoological Journal of the Linnean Society, 188(1), 255-275. https://doi.org/10.1093/zoolinnean/zlz096

Fitzinger, LJFJ. (1872). *Die natürliche Familie der Schuppenthiere (Manes).Sitzungsberichte der kaiserlichen* Akademie der Wissenschaften. https://www.biodiversitylibrary.org/part_231767

Fujita, MK, Leaché, AD, Burbrink, FT, McGuire, JA, & Moritz, C. (2012). Coalescent-based species delimitation in an integrative taxonomy. Trends in ecology & evolution, 27(9), 480-488. https://doi.org/10.1016/j.tree.2012.04.012

Funk, DJ, & Omland, KE. (2003). Species-Level Paraphyly and Polyphyly: Frequency, Causes, and Consequences, with Insights from Animal Mitochondrial DNA. Annual review of ecology, evolution, and systematics, 34(1), 397-423. https://doi.org/10.1146/annurev.ecolsys.34.011802.132421

Gaubert, P, & Antunes, A. (2005). Assessing the taxonomic status of the Palawan pangolin *Manis culionensis* (Pholidota) using discrete morphological characters. Journal of Mammalogy, 86(6), 1068-1074. https://doi.org/10.1644/1545-1542(2005)86[1068:ATTSOT]2.0.CO;2

Gaubert, P, Antunes, A, Meng, H, Miao, L, Peigné, S, Justy, F, Njiokou, F, Dufour, S, Danquah, E, & Alahakoon, J. (2018). The complete phylogeny of pangolins: scaling up resources

for the molecular tracing of the most trafficked mammals on earth. Journal of Heredity, 109(4), 347-359. https://doi.org/10.1093/jhered/esx097

Gaudin, TJ, Emry, RJ, & Wible, JR. (2009). The phylogeny of living and extinct pangolins (Mammalia, Pholidota) and associated taxa: a morphology based analysis. Journal of mammalian evolution, 16, 235-305. https://doi.org/10.1007/s10914-009-9119-9

Gomez, L, Joseph, T, Heinrich, S, Wright, B, & D'Cruze, N. (2023). Illegal trade of pangolins in India with international trade links: an analysis of seizures from 1991 to 2022. European Journal of Wildlife Research, 69(4), 85. https://doi.org/10.1007/s10344-023-01708-9

Goossens, B, Sharma, R, Othman, N, Kun-Rodrigues, C, Sakong, R, Ancrenaz, M, Ambu, LN, Jue, NK, O'Neill, RJ, & Bruford, MW. (2016). Habitat fragmentation and genetic diversity in natural populations of the Bornean elephant: Implications for conservation. Biological Conservation, 196, 80-92. https://doi.org/10.1016/j.biocon.2016.02.008

Goswami, A. (2006). Cranial modularity shifts during mammalian evolution. The American Naturalist, 168(2), 270-280. https://doi.org/10.1086/505758

Gu, T-T, Wu, H, Yang, F, Gaubert, P, Heighton, SP, Fu, Y, Liu, K, Luo, S-J, Zhang, H-R, & Hu, J-Y. (2023). Genomic analysis reveals a cryptic pangolin species. Proceedings of the National Academy of Sciences, 120(40), e2304096120. https://doi.org/10.1073/pnas.2304096120

Guo, C, Jinyao, L, Siyuan, L, Yuze, J, Chunfang, L, Yan, H, Bo, L, Li, L, Songyuan, T, & Yanchun, X. (2022). Coding System and Comparisons of Scales Between Malayan Pangolin(*Manis javanica*) and Chinese Pangolin(*M. pentadactyla*). Chinese Journal of Wildlife, 43(1), 024 －031. https://doi.org/10.19711/j.cnki.issn2310-1490.2022.01.003

Hautier, L, Billet, G, De Thoisy, B, & Delsuc, F. (2017). Beyond the carapace: skull shape variation and morphological systematics of long-nosed armadillos (genus *Dasypus*). PeerJ, 5, e3650. https://doi.org/10.7717/peerj.3650

Hawkins, MT, Leonard, JA, Helgen, KM, McDonough, MM, Rockwood, LL, & Maldonado, JE. (2016). Evolutionary history of endemic Sulawesi squirrels constructed from UCEs and mitogenomes sequenced from museum specimens. BMC evolutionary biology, 16, 1-16. https://doi.org/10.1186/s12862-016-0650-z

He, K, & Jiang, X. (2014). Sky islands of southwest China. I: an overview of phylogeographic patterns. Chinese Science Bulletin, 59, 585-597. https://doi.org/10.1007/s11434-013-0089-1

Heighton, SP, Allio, R, Murienne, J, Salmona, J, Meng, H, Scornavacca, C, Bastos, AD, Njiokou, F, Pietersen, DW, & Tilak, M-K. (2023). Pangolin genomes offer key insights and resources for the world's most trafficked wild mammals. Molecular biology and evolution, 40(10), msad190.

Hinckley, A, Hawkins, MT, Maldonado, JE, & Leonard, JA. (2023). Evolutionary history and patterns of divergence in three tropical east Asian squirrels across the Isthmus of Kra. Journal of Biogeography, 50(6), 1090-1102. https://doi.org/10.1111/jbi.14598

Hinckley, A, Maldonado, JE, Tamura, N, Leonard, JA, & Hawkins, MT. (2024). Lost in synonymy: Integrative species delimitation reveals two unrecognized species of Southern Asian tree squirrels (Rodentia: *Sciuridae: Callosciurinae*). Vertebrate Zoology, 74, 683-707. https://doi.org/10.3897/vz.74.e133467

Hodgson, BH. (1836). New Mammals in Nipdlese Catalogue. The journal of the Asiatic Society of Bengal, V, 234-235. https://www.biodiversitylibrary.org/bibliography/51678

Hogan, F, Wedrowicz, F, Pd. Khatiwada, A, Dev Joshi, J, Wasser, S, & Wright, W. (2025). Genetic evidence reveals distinct lineage of Chinese pangolin in Nepal: insights from scat and blood samples for conservation and wildlife forensics. Ecology and Evolution, 15(2), e70982. https://doi.org/10.1002/ece3.70982

Hu, J-Y, Hao, Z-Q, Frantz, L, Wu, S-F, Chen, W, Jiang, Y-F, Wu, H, Kuang, W-M, Li, H, & Zhang, Y-P. (2020a). Genomic consequences of population decline in critically endangered pangolins and their demographic histories. National Science Review, 7(4), 798-814. https://doi.org/10.1093/nsr/nwaa031

Hu, Y, Thapa, A, Fan, H, Ma, T, Wu, Q, Ma, S, Zhang, D, Wang, B, Li, M, & Yan, L. (2020b). Genomic evidence for two phylogenetic species and long-term population bottlenecks in red pandas. Science Advances, 6(9), eaax5751. https://doi.org/10.1126/sciadv.aax575

Igado, O, Adekanmbi, J, Adebayo, M, Sulaimon, O, & Osundina, O. (2020). Facial and Body Morphometric Indices of the Arboreal African Pangolin (*Manis tricuspis*): Anthropometric Tools in Describing the Pangolin: Facial and biometric indices of the African pangolin. Sahel Journal of Veterinary Sciences, 17(3), 28-33. https://doi.org/10.54058/saheljvs.v17i3.122

Imam, A, Bhagwandin, A, Ajao, MS, Spocter, MA, Ihunwo, AO, & Manger, PR. (2018). The brain of the tree pangolin (*Manis tricuspis*). II. The olfactory system. Journal of Comparative Neurology, 526(16), 2548-2569. https://doi.org/10.1002/cne.24510

IUCN SSC Pangolin Specialist Group, IUCN SSC Asian Species Action Partnership, Wildlife Reserves Singapore, IS, & Group., CPS. (2018). *Regional Sunda Pangolin (Manis javanica) Conservation Strategy 2018-2028. IUCN SSC*

Pangolin Specialist Group. https://pangolinsg.org/wp-content/uploads/sites/4/2020/01/Pangolin-SG-et-al_2018_Regional-Sunda-pangolin-conservation-strategy-2018-2028.pdf

Katoh, K, & Standley, DM. (2013). MAFFT multiple sequence alignment software version 7: improvements in performance and usability. Molecular biology and evolution, 30(4), 772-780. https://doi.org/10.1093/molbev/mst010

Koju, NP. (2018). *Abundance and phylogenetic status of Chinese Pangolin (Manis pentadactyla) from Kathmandu valley, Nepal*.

Koju, NP, He, K, Chalise, MK, Ray, C, Chen, Z, Zhang, B, Wan, T, Chen, S, & Jiang, X. (2017). Multilocus approaches reveal underestimated species diversity and inter-specific gene flow in pikas (*Ochotona*) from southwestern China. Molecular Phylogenetics and Evolution. https://doi.org/https://doi.org/10.1016/j.ympev.2016.11.005

Koju, NP, & Tamang, BM. (2025). Illegal Wildlife Trade in Kathmandu Valley: A Hub of Biodiversity Crime. Ecology and Evolution (unpublished).

Korunes, KL, & Samuk, K. (2021). pixy: Unbiased estimation of nucleotide diversity and divergence in the presence of missing data. Molecular ecology resources, 21(4), 1359-1368. https://doi.org/10.1111/1755-0998.13326

Lehman, SM, Fleagle, JG, Meijaard, E, & Groves, CP. (2006). The geography of mammals and rivers in mainland Southeast Asia. In Primate Biogeography. Developments in Primatology: Progress and Prospects (pp. 305-329). Springer. https://doi.org/10.1007/0-387-31710-4_11

Leonard, JA, den Tex, RJ, Hawkins, MT, Muñoz‐Fuentes, V, Thorington, R, & Maldonado, JE. (2015). Phylogeography of vertebrates on the Sunda Shelf: a multi‐species comparison. Journal of Biogeography, 42(5), 871-879. https://doi.org/10.1111/jbi.12465

Li, H, & Durbin, R. (2011). Inference of human population history from individual whole-genome sequences. Nature, 475(7357), 493-496. https://doi.org/10.1038/nature10231

Li, H, Handsaker, B, Wysoker, A, Fennell, T, Ruan, J, Homer, N, Marth, G, Abecasis, G, Durbin, R, & Subgroup, GPDP. (2009). The sequence alignment/map format and SAMtools. bioinformatics, 25(16), 2078-2079. https://doi.org/10.1093/bioinformatics/btp352

Li, J, Guo, C, Xie, M, Wang, K, Wang, X, Zou, B, Hou, F, Ran, C, Bi, S, & Xu, Y. (2024). Genomic signatures of sensory adaptation and evolution in pangolins. BMC genomics, 25(1), 1-13. https://doi.org/10.1186/s12864-024-11063-x

Li, Z, Fan, H, Liao, Z, Wang, Y, & Wei, F. (2025). Global spatiotemporal patterns of demographic fluctuations in terrestrial vertebrates during the Late Pleistocene. Science Advances, 11(21), eadq3938. https://doi.org/10.1126/sciadv.adq3938

Louys, J, & Meijaard, E. (2010). Palaeoecology of Southeast Asian megafauna‐bearing sites from the Pleistocene and a review of environmental changes in the region. Journal of Biogeography, 37(8), 1432-1449. https://doi.org/10.1111/j.1365-2699.2010.02297.x

Ma, T, Tarasov, PE, Huang, K, Leipe, C, Man, M, & Zheng, Z. (2022). Intensified climate drying and cooling during the last glacial culmination (20.8–17.5 cal ka BP) in the south-eastern Asian monsoon domain inferred from a high-resolution pollen record. Quaternary Science Reviews, 278, 107371. https://doi.org/10.1016/j.quascirev.2022.107371

Malinsky, M, Matschiner, M, & Svardal, H. (2021). Dsuite‐Fast D‐statistics and related admixture evidence from VCF files. Molecular ecology resources, 21(2), 584-595. https://doi.org/10.1111/1755-0998.13265

Martin, JM, Buckley, JY, Connelly, E, Hywood, L, Lacey, LM, Ruden, RM, Ruhagazi, D, & Wearn, A. (2024). The Pangolin Universal Notching System: a scale-marking methodology for pangolins. Oryx, 1-7. https://doi.org/1017/S0030605324000656

McKenna, A, Hanna, M, Banks, E, Sivachenko, A, Cibulskis, K, Kernytsky, A, Garimella, K, Altshuler, D, Gabriel, S, & Daly, M. (2010). The Genome Analysis Toolkit: a MapReduce framework for analyzing next-generation DNA sequencing data. Genome research, 20(9), 1297-1303. https://doi.org/10.1101/gr.107524.110

McQuillan, R, Leutenegger, A-L, Abdel-Rahman, R, Franklin, CS, Pericic, M, Barac-Lauc, L, Smolej-Narancic, N, Janicijevic, B, Polasek, O, & Tenesa, A. (2008). Runs of homozygosity in European populations. The American journal of human genetics, 83(3), 359-372. https://doi.org/10.1016/j.ajhg.2008.08.007

Meng, G, Li, Y, Yang, C, & Liu, S. (2019). MitoZ: a toolkit for animal mitochondrial genome assembly, annotation and visualization. Nucleic acids research, 47(11), e63-e63. https://doi.org/10.1093/nar/gkz173.

Morenikeji, O, Omotosho, O, Jarikre, T, Emikpe, B, Fawole, E, Adeyefa, A, & Olapade, B. (2022). Morphometric characterisation of white-bellied pangolins rescued from trade for conservation in Nigeria. Emerging Animal Species, 1, 100018. https://doi.org/10.1016/j.eas.2022.100018

Nijman, V, Zhang, MX, & Shepherd, CR. (2016). Pangolin trade in the Mong La wildlife market and the role of Myanmar in the smuggling of pangolins into China. Global Ecology and Conservation, 5, 118-126. https://doi.org/10.1016/j.gecco.2015.12.003

Padial, JM, Miralles, A, De la Riva, I, & Vences, M. (2010). The integrative future of taxonomy. Frontiers in zoology, 7, 1-14. https://doi.org/10.1186/1742-9994-7-16

Patterson, N, Price, AL, & Reich, D. (2006). Population structure and eigenanalysis. PLoS genetics, 2(12), e190. https://doi.org/10.1371/journal.pgen.0020190

Purcell, S, Neale, B, Todd-Brown, K, Thomas, L, Ferreira, MA, Bender, D, Maller, J, Sklar, P, De Bakker, PI, & Daly, MJ. (2007). PLINK: a tool set for whole-genome association and population-based linkage analyses. The American journal of human genetics, 81(3), 559-575. https://doi.org/10.1086/519795

Rambaut, A, Suchard, M, & Xie, D. (2017). Drummond AJ. 2014. Tracer v1. 6. In.

Rieseberg, LH, & Burke, JM. (2001). The biological reality of species: gene flow, selection, and collective evolution. Taxon, 50(1), 47-67. https://doi.org/10.2307/1224511

Schlick-Steiner, BC, Steiner, FM, Seifert, B, Stauffer, C, Christian, E, & Crozier, RH. (2010). Integrative taxonomy: a multisource approach to exploring biodiversity. Annual review of entomology, 55(1), 421-438. https://doi.org/10.1146/annurev-ento-112408-085432

Shrestha, A, Bhattarai, S, Shrestha, B, & Koju, NP. (2021). Factors influencing the habitat choice of pangolins (*Manis* spp.) in low land of Nepal. Ecology and Evolution, 11(21), 14689-14696.

Shrestha, S, Bashyal, A, Dhakal, A, McGreevy Jr, TJ, Buffum, B, Joshi, J, Chaudhary, HK, & Khanal, SN. (2020). Mitochondrial DNA analysis of critically endangered Chinese Pangolins (*Manis pentadactyla*) from Nepal. Mitochondrial DNA Part B, 5(3), 3257-3261.

Smith, SA, Brown, JW, & Walker, JF. (2018). So many genes, so little time: a practical approach to divergence-time estimation in the genomic era. Plos one, 13(5), e0197433. https://doi.org/10.1371/journal.pone.0197433

Sulaiman, MH, Azmi, WA, Hassan, M, & Chong, JL. (2017). Current updates on the morphological measurements of the Malayan pangolin (*Manis javanica*). Folia Zoologica, 66(4), 262-266. https://doi.org/10.25225/fozo.v66.i4.a8.2017

Thapa, P, Khatiwada, AP, Nepali, SC, & Paudel, S. (2014). Distribution and conservation status of Chinese pangolin (*Manis pentadactyla*) in Nangkholyang VDC, Taplejung, eastern Nepal. American Journal of Zoological Research, 2(1), 16-21.

Toews, DP, & Brelsford, A. (2012). The biogeography of mitochondrial and nuclear discordance in animals. Molecular ecology, 21(16), 3907-3930. https://doi.org/10.1111/j.1365-294X.2012.05664.x

Van Elst, T, Sgarlata, GM, Schüßler, D, Tiley, GP, Poelstra, JW, Scheumann, M, Blanco, MB, Aleixo-Pais, IG, Rina Evasoa, M, & Ganzhorn, JU. (2025). Integrative taxonomy clarifies the evolution of a cryptic primate clade. Nature Ecology & Evolution, 9(1), 57-72. https://doi.org/10.1038/s41559-024-02547-w

Wang, Q, Lan, T, Li, H, Sahu, SK, Shi, M, Zhu, Y, Han, L, Yang, S, Li, Q, & Zhang, L. (2022). Whole-genome resequencing of Chinese pangolins reveals a population structure and provides insights into their conservation. Communications Biology, 5(1), 821. https://doi.org/10.1038/s42003-022-03757-3

Wangmo, LK, Ghosh, A, Dolker, S, Joshi, BD, Sharma, LK, & Thakur, M. (2025). Indo-Burmese pangolin (*Manis indoburmanica*): a novel phylogenetic species of pangolin evolved in Asia. Mammalian biology, 1-8. https://doi.org/10.1007/s42991-024-00475-7

Wei, S, Fan, H, Zhou, W, Huang, G, Hua, Y, Wu, S, Wei, X, Chen, Y, Tan, X, & Wei, F. (2024). Conservation genomics of the critically endangered Chinese pangolin. Science China Life Sciences, 1-11. https://doi.org/10.1007/s11427-023-2540-y

Wilson, DE, & Mittermeier, RA. (2018). *Handbook of the mammals of the world: vol. 8: insectivores, sloths and colugos*. Lynx Edicions.

Wu, S, Naifa, L, Zhang Yingmei, Zhi, O, & Hai, C. (2005). Measurement and Comparison of Skull Variables in Chinese Pangolin and Malayan Pangolin. ACTA THERIOLOGICA SINICA, 24(3), 211. https://doi.org/10.16829/j.slxb

Xie, X, Ye, H, Cai, X, Li, C, Li, F, Tian, E, & Chao, Z. (2021). DNA mini-barcodes, a potential Weapon for Conservation and combating illegal trade of pangolin. Tropical Conservation Science, 14, 19400829211017361. https://doi.org/10.1177/1940082921101736

Yu, G, Wang, L-G, Han, Y, & He, Q-Y. (2012). clusterProfiler: an R package for comparing biological themes among gene clusters. Omics: a journal of integrative biology, 16(5), 284-287. https://doi.org/10.1089/omi.2011.0118

Zhang, F, Wu, S, & Cen, P. (2022). The past, present and future of the pangolin in Mainland China. Global Ecology and Conservation, 33, e01995. https://doi.org/10.1016/j.gecco.2021.e01995

Zhang, F, Yu, Y, Wu, S, Mahmood, A, Yu, J, & Min, Y. (2020). Reducing pangolin demand by understanding motivations for human consumption in Guangdong, China. Frontiers in Ecology and Evolution, 8, 574161. https://doi.org/10.3389/fevo.2020.574161

Zhang, M, Gouveia, A, Qin, T, Quan, R, & Nijman, V. (2017). Illegal pangolin trade in northernmost Myanmar and its links to India and China. Global Ecology and Conservation, 10, 23-31. https://doi.org/10.1016/j.gecco.2017.01.006

Zijlstra, JS. (2025). Manis aurita Hodgson 1837 as a valid species of pangolin: a comment to Wangmo et al.(2025). Mammalian biology, 1-3. https://doi.org/10.1007/s42991-025-00495-x

Zoological Society of London. (2014). *Plight of the pangolin: all eight species to move up EDGE list. EDGE of Existence*. Retrieved September 12 from https://www.edgeofexistence.org/blog/plight-of-the-pangolin-all-eight-species-move-up-edge-list/

Figures

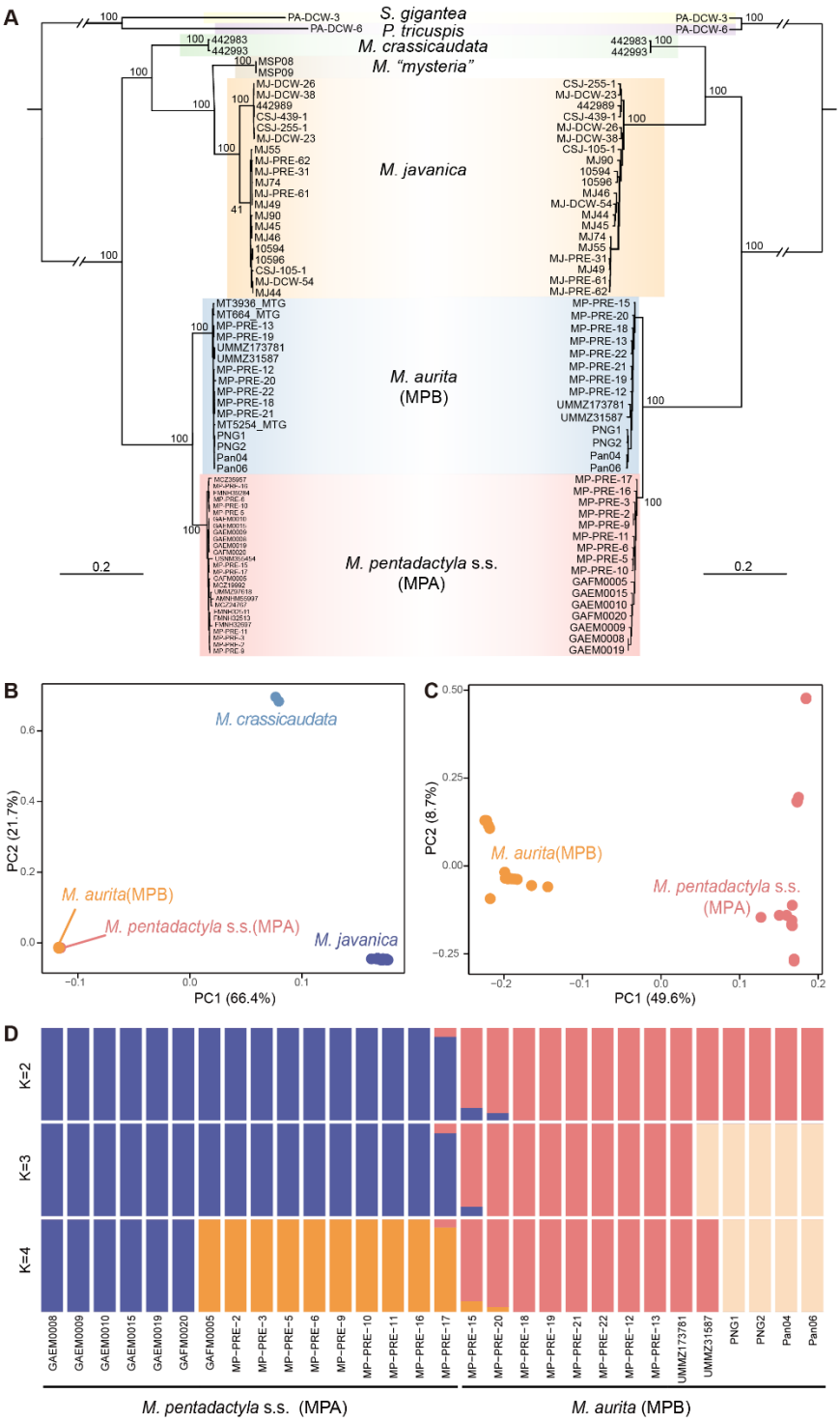

Figure 1. Phylogenetic relationships and population structure of pangolins. (A) Maximum likelihood (ML) phylogenies based on mitochondrial genomes (left) and autosomal SNPs (right). (B) Principal Component Analysis (PCA) of 52 individuals from four *Manis* species. (C) PCA focused on 30 individuals, illustrating the genetic separation between *M. pentadactyla* s.s. and *M. aurita*. (D) Population structure of *M. pentadactyla* s.s. and *M. aurita* inferred by ADMIXTURE for K=2 to K=4 ancestral populations. Each vertical bar represents an individual, and colors correspond to inferred ancestry proportions.

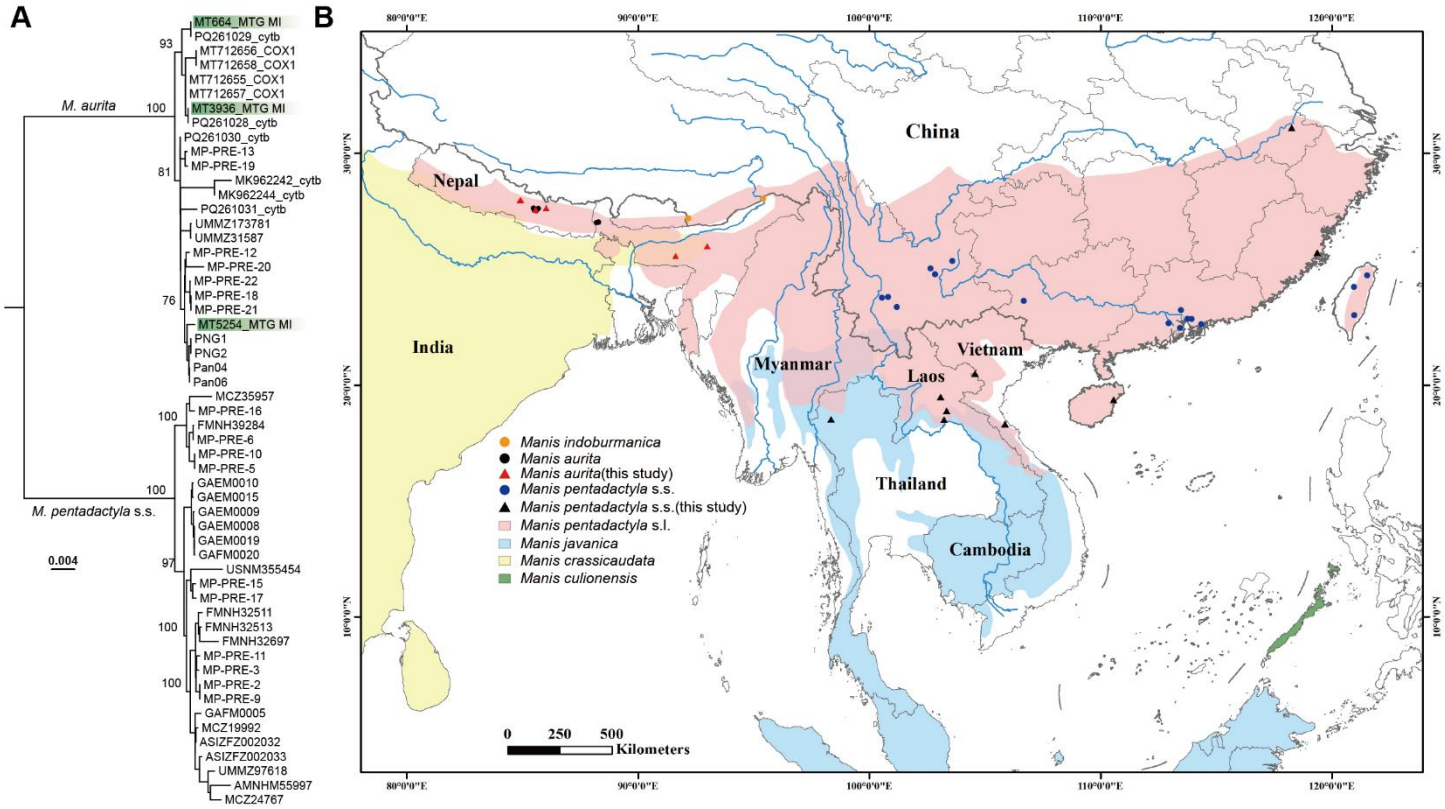

Figure 2. Mitochondrial phylogeny and geographic distribution of *Manis pentadactyla* sensu lato. (A) Maximum likelihood phylogeny constructed from an expanded dataset including complete mitogenomes and partial *CYTB* and *COX1* sequences incorporating public data to place additional samples, including those described as *M. indoburmanica* (MI). (B) Geographic distribution map showing the provenance for *M. pentadactyla* s.s. and *M. aurita* (including *M. indoburmanica*), based on samples with reliable locality information (Table S1).

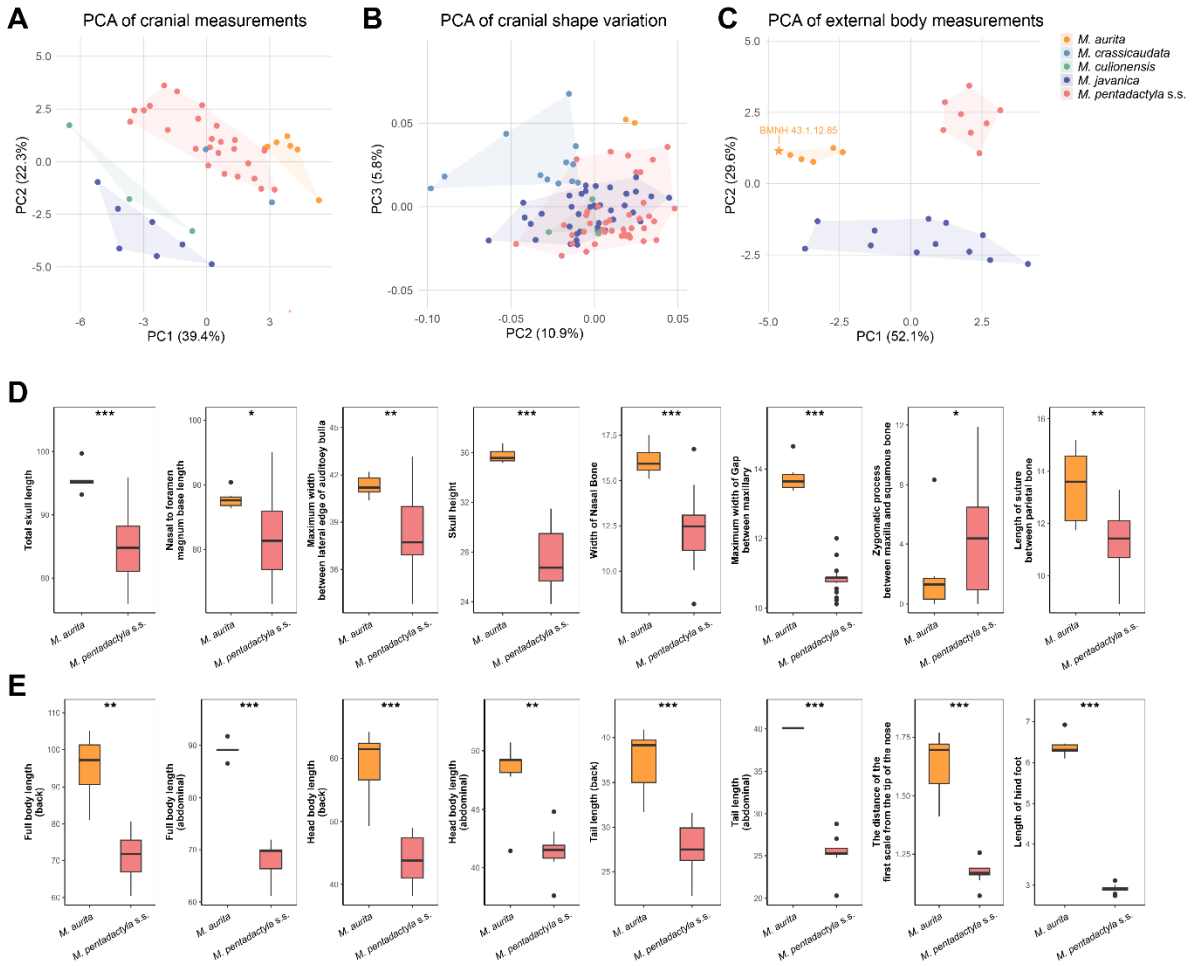

Figure 3. Morphometric analyses reveal consistent differentiation between *M. pentadactyla* s.s. and *M. aurita*. (A) First and second principal components from a PCA of 20 linear cranial measurements. (B) Second and third principal components from a PCA of cranial shape variation derived from 75 3D geometric morphometric landmarks. (C) First and second principal components from a PCA of 14 external body measurements. (D-E) Univariate boxplots comparing key cranial and external (E) measurements between the two species. Boxes show the interquartile range (IQR) with the median as a horizontal line, and whiskers extend to 1.5 times the IQR. Statistical significance from Student's t-tests is denoted as: * $P < 0.05$; ** $P < 0.01$; *** $P < 0.001$. The y-axis represents measurement values, with units in millimeters for (D) and centimeters for (E). Additional results of PCA and boxplots can be found in table S5, S6, S7, S8, figure S4, S9, S10.

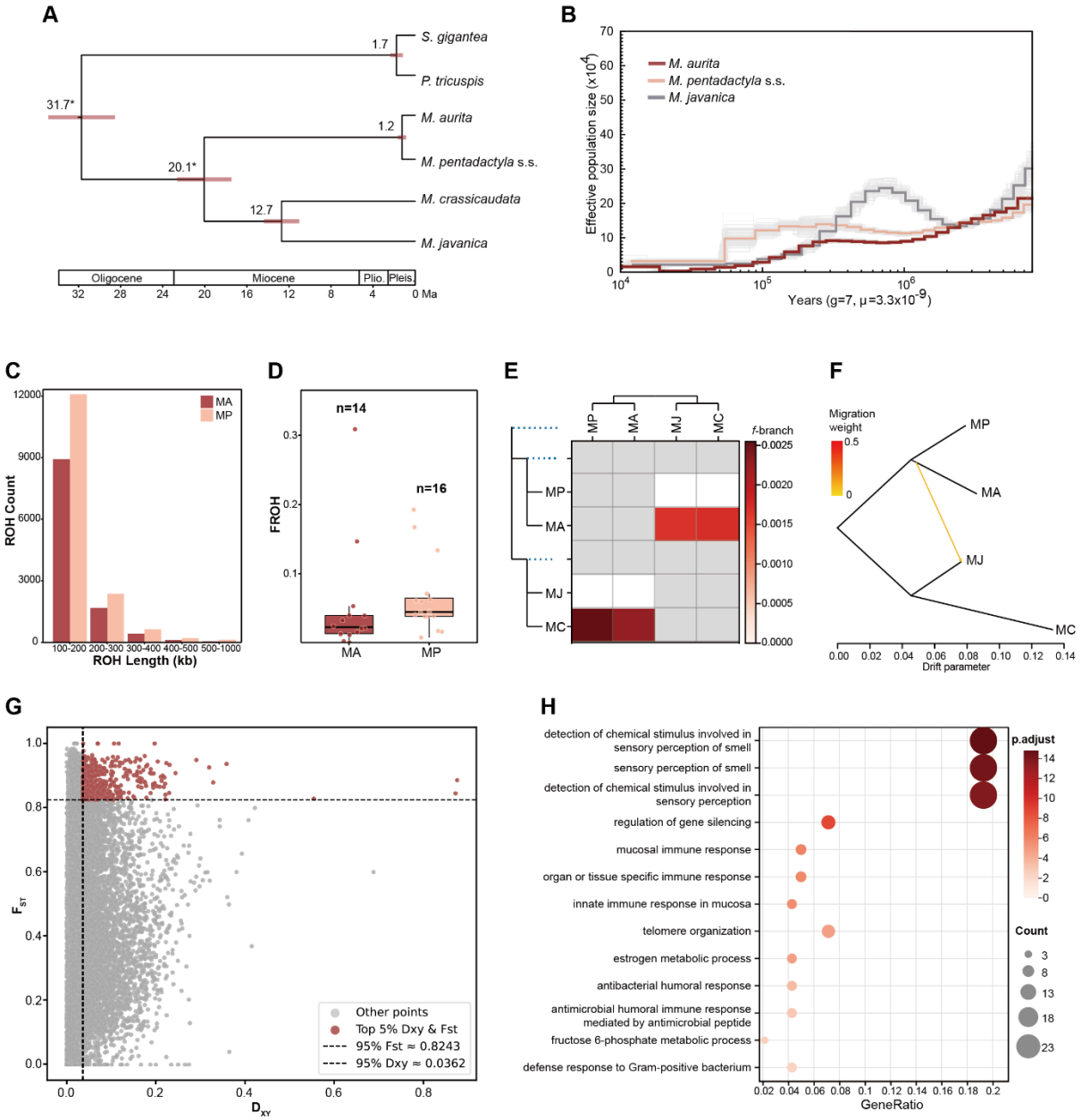

Figure 4. Divergence time, demographic dynamics, and genomic divergence of *Manis* species. (A) Divergence time estimates for pangolins based on 200 clock-like single-copy genes, inferred using *BEAST3. Numbers at nodes represent mean age estimates in millions of years (Ma). Asterisks indicate nodes used for calibration. (B) Historical effective population size (N_e) trajectories for *three species* inferred using PSMC. Shaded areas represent 100 bootstrap replicates. (C-D) Comparison of recent inbreeding levels between *M. aurita* (MA) and *M. pentadactyla* s.s. (MP), showing (C) the distribution of Runs of Homozygosity (ROH) lengths and (D) the genome-wide fraction of ROH (F_{ROH}). (E-F) Interspecific gene flow analyses among four *Manis* species. MC: *M. crassicaudata*, MJ: *Manis javanica*. (E) Heatmap of Dsuite f-branch statistics, where warmer colors indicate stronger signals of admixture on a given branch. (F) TreeMix population graph showing inferred drift and a migration event (arrow). (G-H) Genomic differentiation between *M. aurita* and *M. pentadactyla* s.s. (G) Manhattan plot of FST and dXY values, with dashed lines indicating the 95% outlier thresholds used to define genomic islands of divergence. (H) Gene Ontology (GO) enrichment analysis of genes within the identified genomic islands, with dot size corresponding to gene count and color to statistical significance (p.adjust).

Supplementary figures

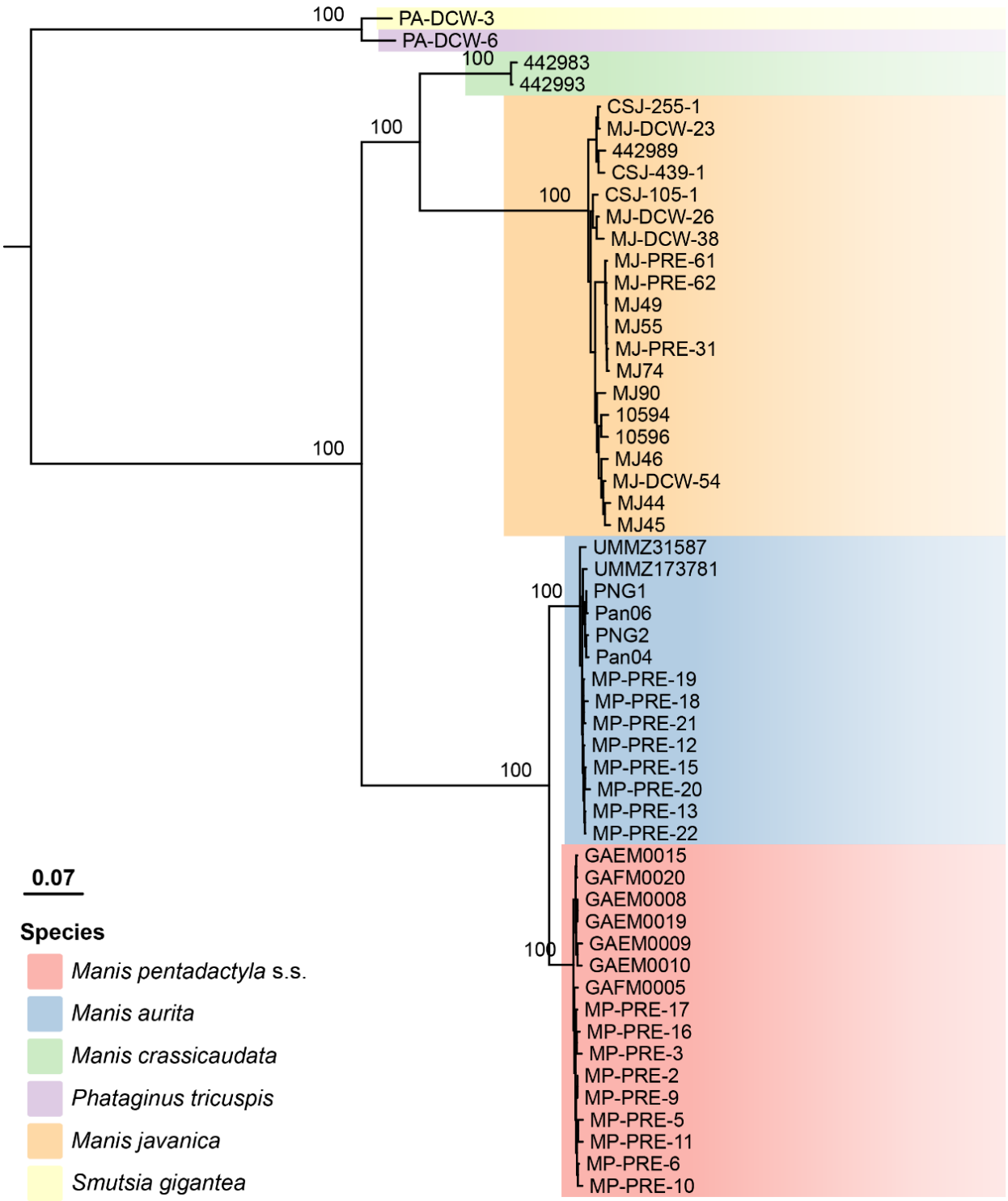

Fig S1. Phylogenetic Inference Based on Sex Chromosome SNPs Using Maximum Likelihood in IQ-TREE with 1000 Bootstrap Replicates.

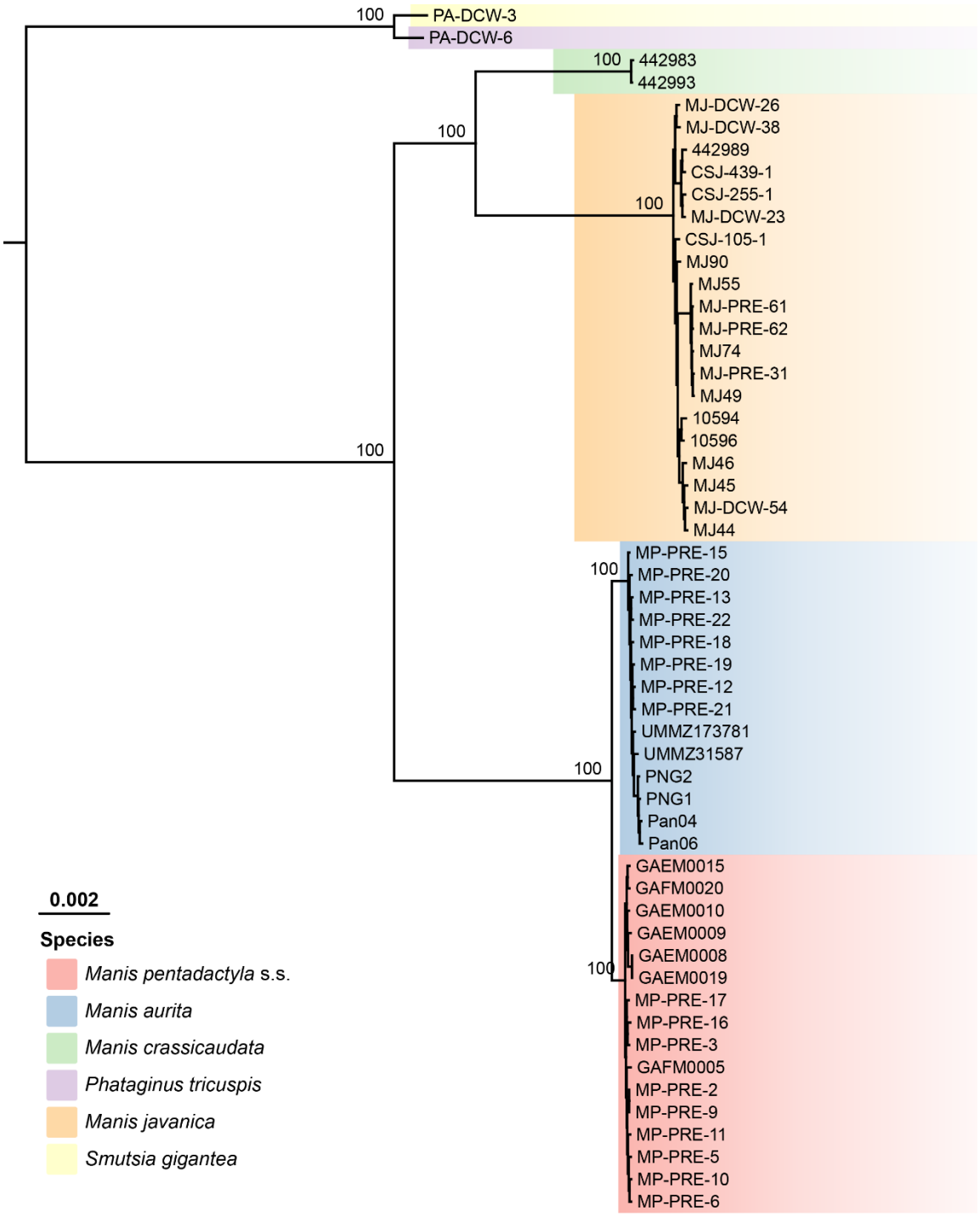

Fig S2. Phylogenetic tree reconstructed using maximum likelihood based on 7,852 single-copy orthologous genes, inferred with IQ-TREE and supported by 1,000 bootstrap replicates.

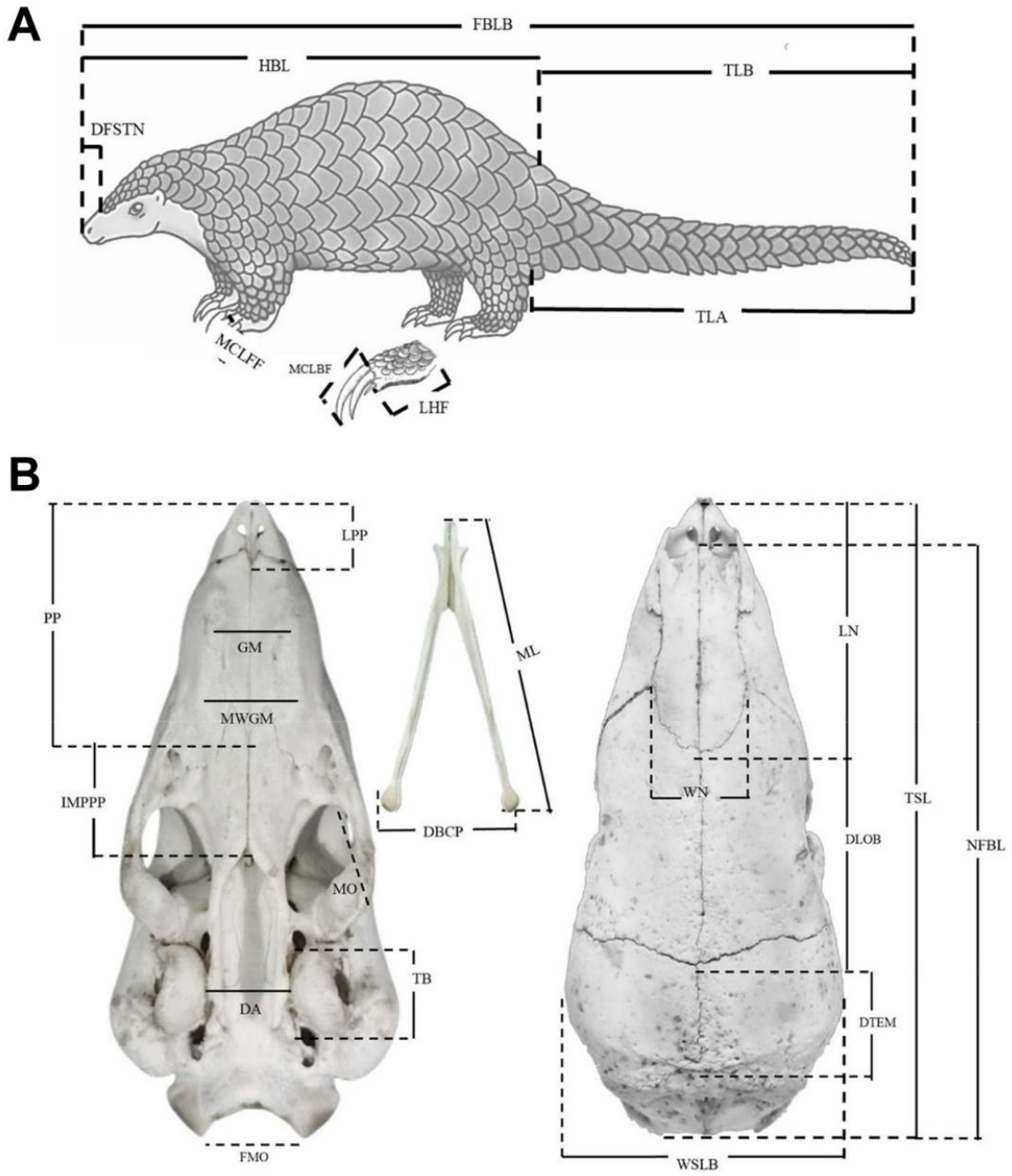

Fig 13.Illustration of measurement parameters for pangolin body and skull. (A) Body measurement traits of pangolin. (B) Skull measurement traits on ventral and dorsal views.

Note: Total skull length (TSL), Nasal to foramen magnum base length (NFBL), Premaxilla to palatine (PP), Tymapanic bulla (TB) (left), Maximum width between lateral edge of auditory bulla (WSLB), Skull height (H), Width of Nasal Bone (WN), Length of Nasal Bone (LN), Gap between maxillary (dorsal) (GM), Maximum width of Gap between maxillary (MWGM), Maximal length of orbit (MO), Distance between auditory bulla (DA), Length of suture between parietal bone (DTEM), Length of suture between frontal bone (DLOB), Zygomatic process between maxilla and squamous bone (ZMS),Length of foremen Magnum occipitals(FMO), Mandible length(ML), The distance between condylar process (DBCP), Length of palatal process of premaxilla (LPP), Intersection between maxilla and palatine sutures to most posterior point of the palatine sutures (IMPP).

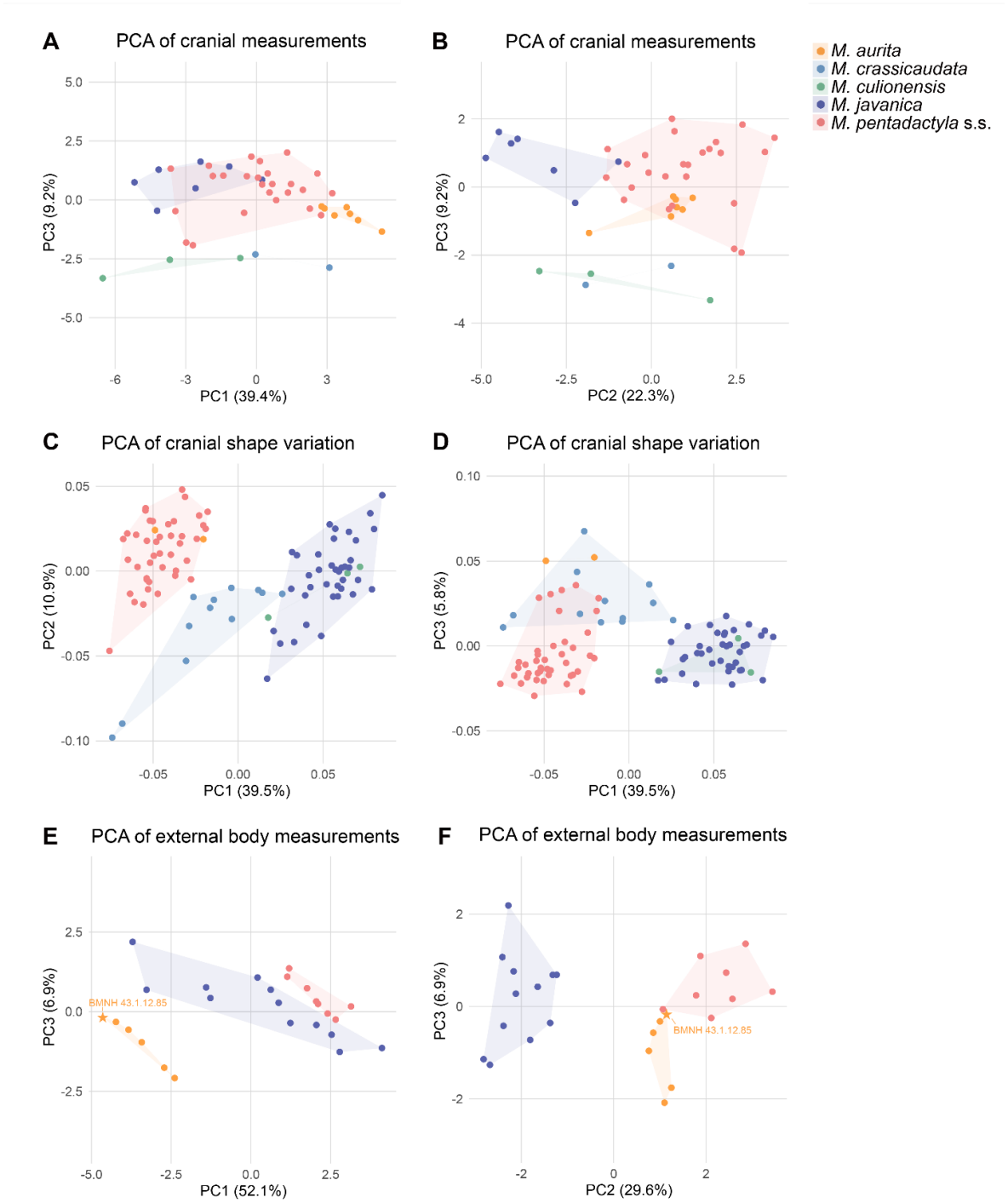

Fig S4. Principal component analyses (PCA) of *Manis* specimens based on different morphological datasets. (A–B) PCA based on cranial measurements. **(C–D)** PCA based on cranial shape variation. **(E–F)** PCA based on external body measurements.

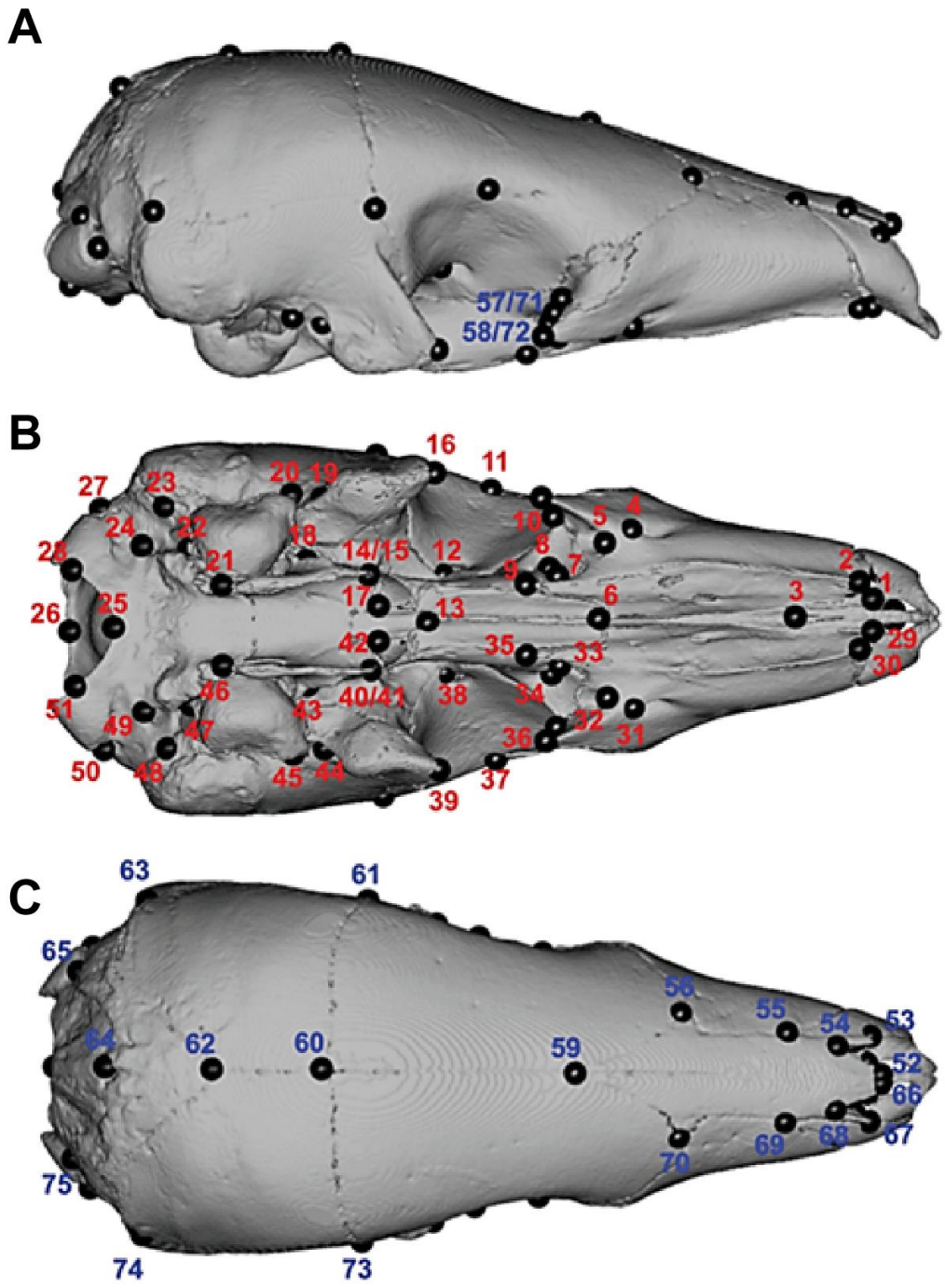

Fig S5. Landmarks digitized on the skull of pangolin. (A) Lateral view, **(B)** ventral view, and **(C)** dorsal view of the skull showing digitized landmarks. Red and blue numbers represent landmarks placed on the ventral and dorsal sides, respectively. Adapted from Ferreira-Cardoso et al. (2020).

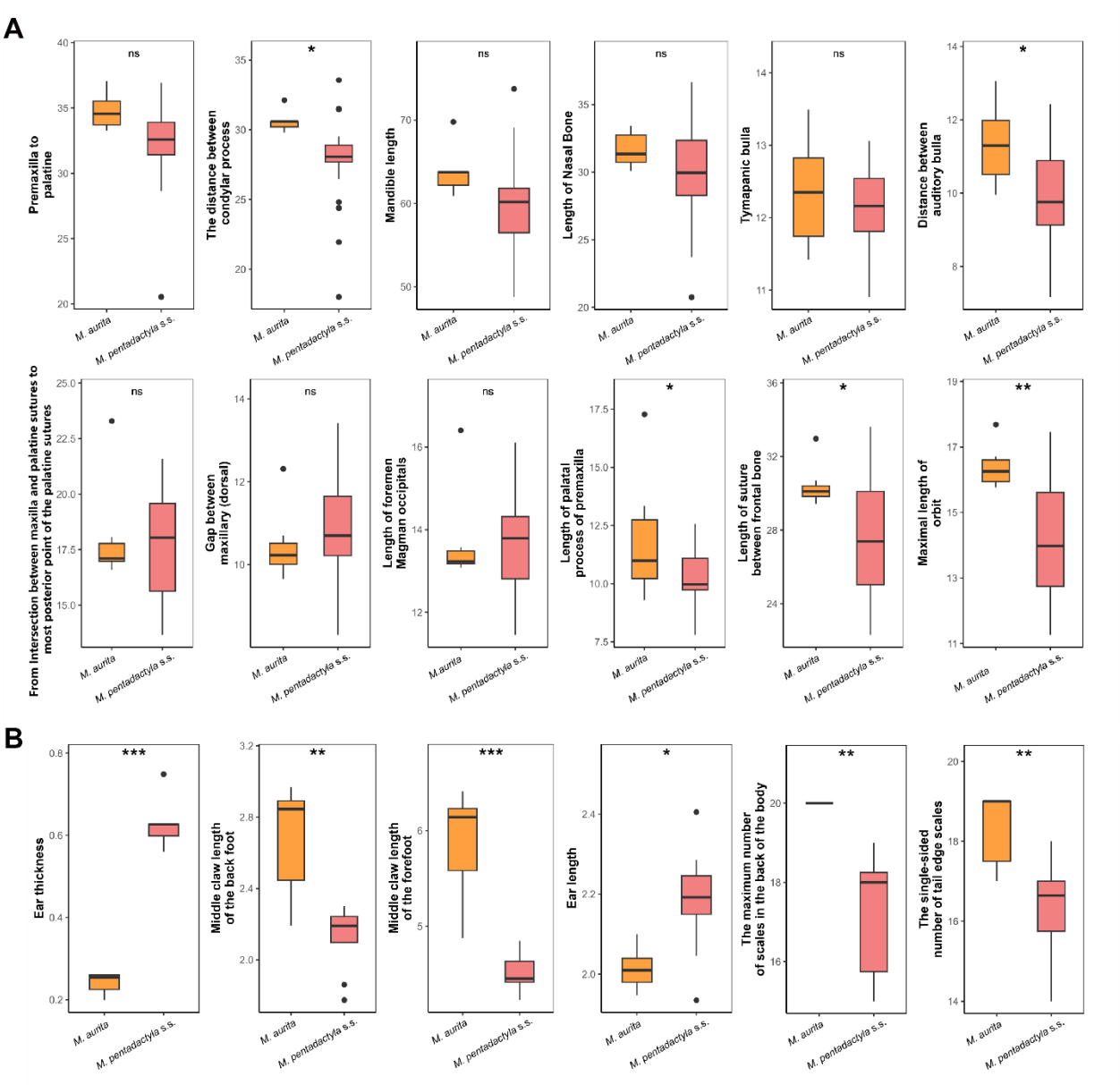

Fig S6. Boxplots comparing cranial and external measurements between *M. pentadactyla* s.s. and *M. aurita*. (A) Boxplots of cranial measurements. **(B)** Boxplots of external body measurements. Boxes show the interquartile range (IQR) with the median as a horizontal line, and whiskers extend to 1.5 times the IQR. Statistical significance from Student's t-tests is denoted as: * $P < 0.05$; ** $P < 0.01$; *** $P < 0.001$. The y-axis represents the measurement values. For **(A)**, all values are in millimeters. For **(B)**, most measurements are in centimeters, except for the maximum number of scales on the back and the single-sided number of tail edge scales, which are expressed as counts (number of scales).

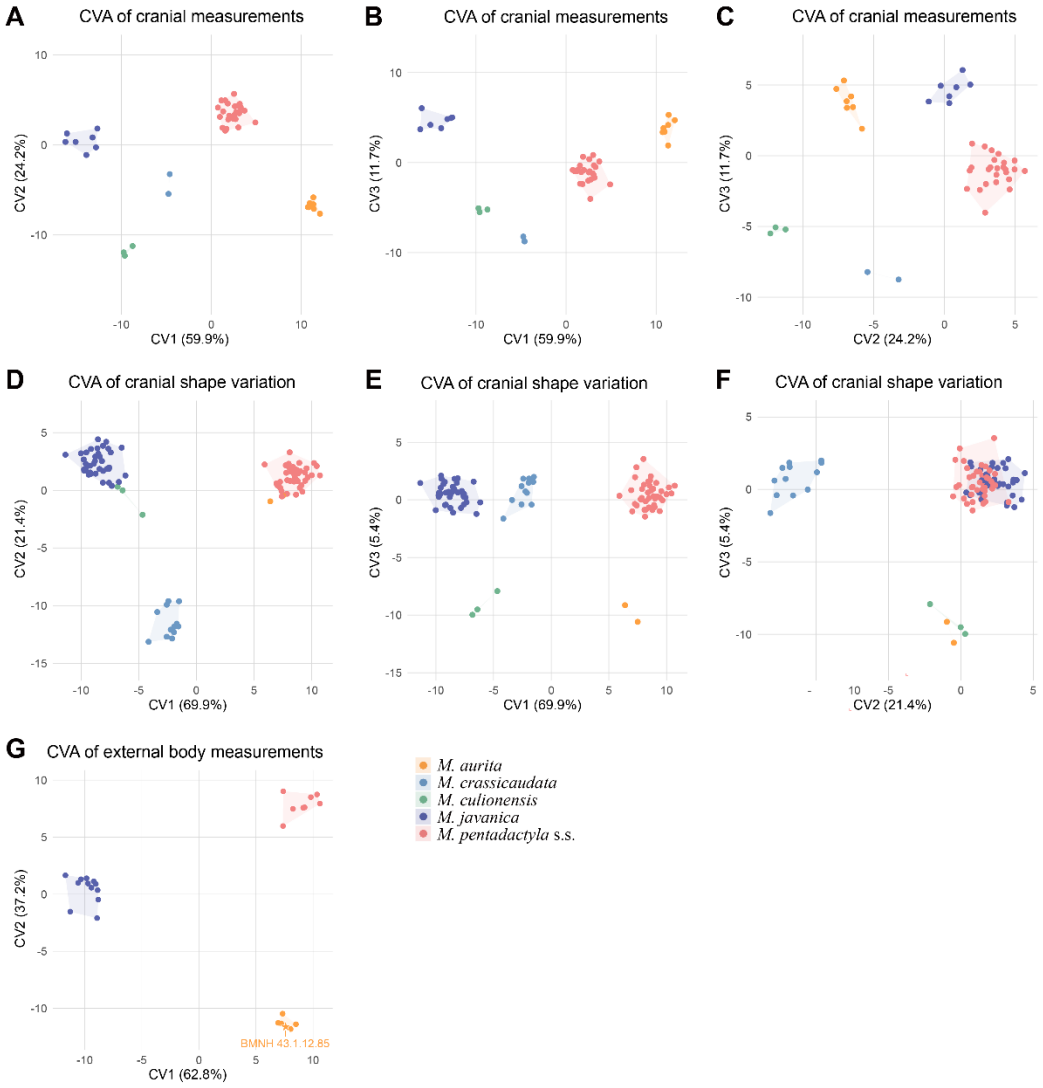

Fig S7. **Canonical variate analyses (CVA) of *Manis* specimens based on different morphological datasets. (A–C)** CVA based on cranial measurements. **(D–F)** CVA based on cranial shape variation. **(G)** CVA based on external body measurements.

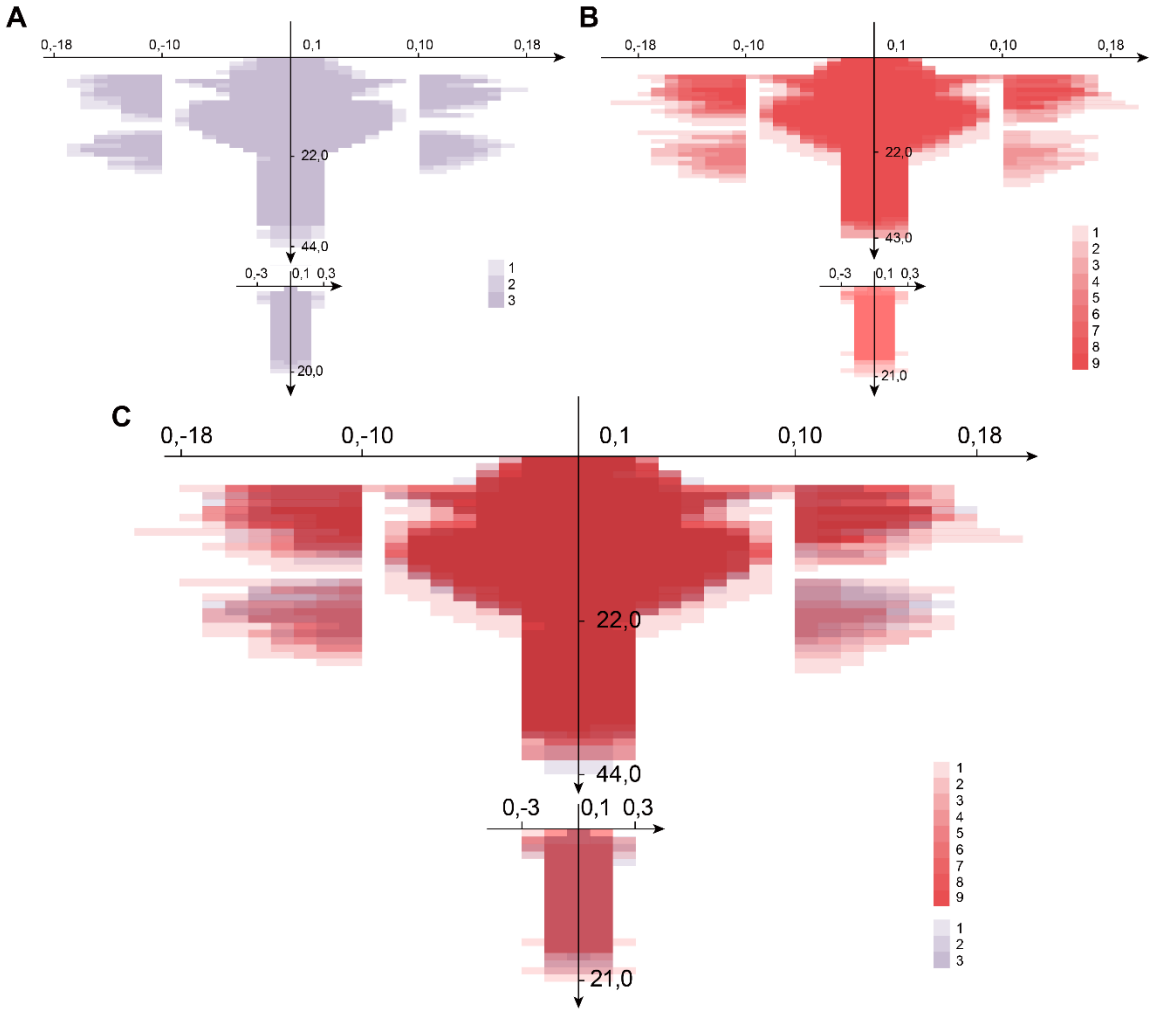

Fig S8. Heat maps showing scale patterns and distribution in *M. pentadactyla* s.s. and *M. aurita*. (A) Heat map of scale pattern in *M. aurita*. **(B)** Heat map of scale pattern in *M. pentadactyla* s.s. **(C)** Comparative heat map of scale distribution between the two species.

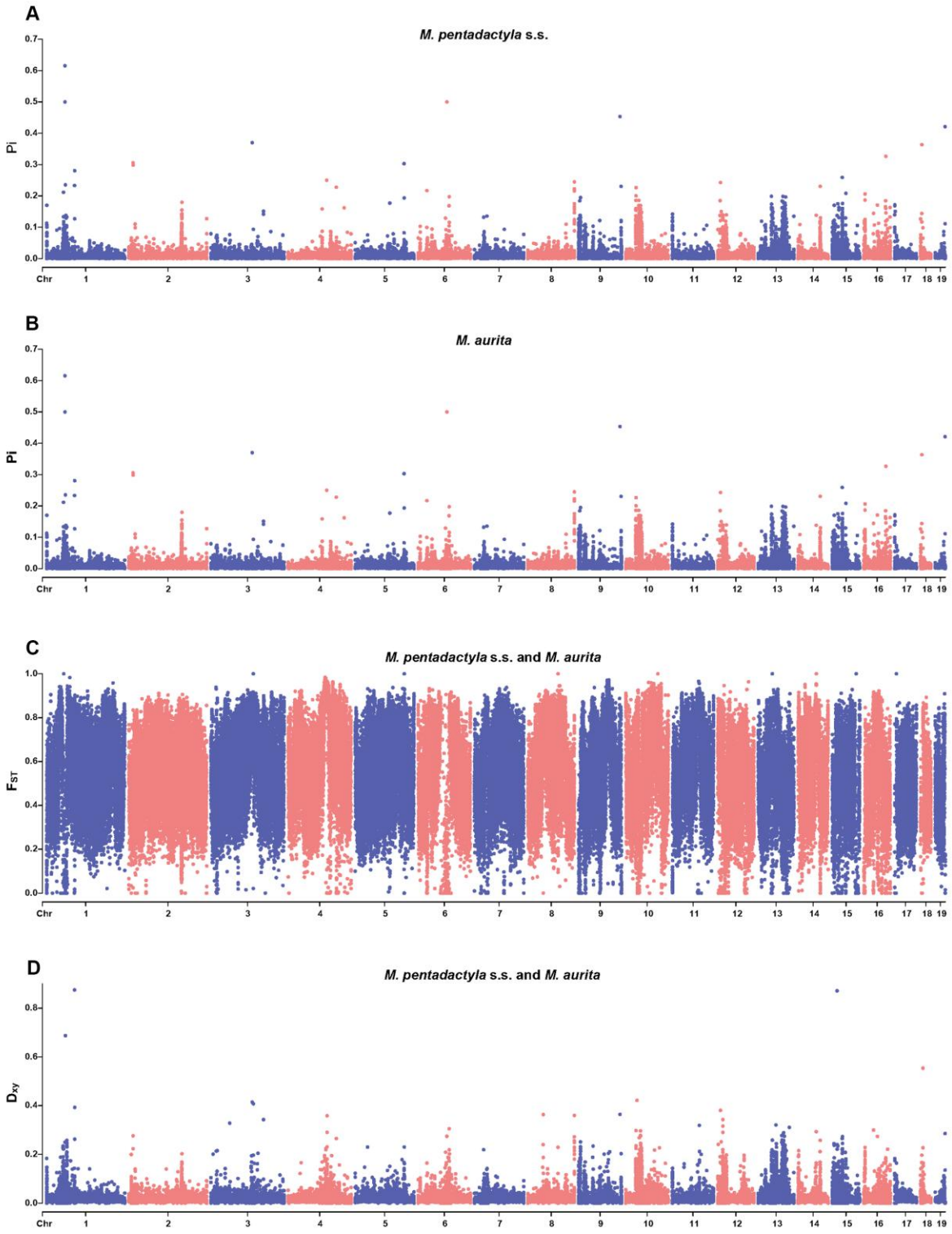

Fig S9. **Genetic diversity analysis based on 20 kb window size using pixy.** (**A**) *M. pentadactyla*'s Nucleotide Diversity (π). (**B**) *M. aurtita*'s Nucleotide Diversity (π). (**C**) Population Differentiation (Fst) between *M. pentadactyla* and *M. aurtita.* (**D**) Absolute Divergence (Dxy) between *M. pentadactyla* and *M. aurtita*.

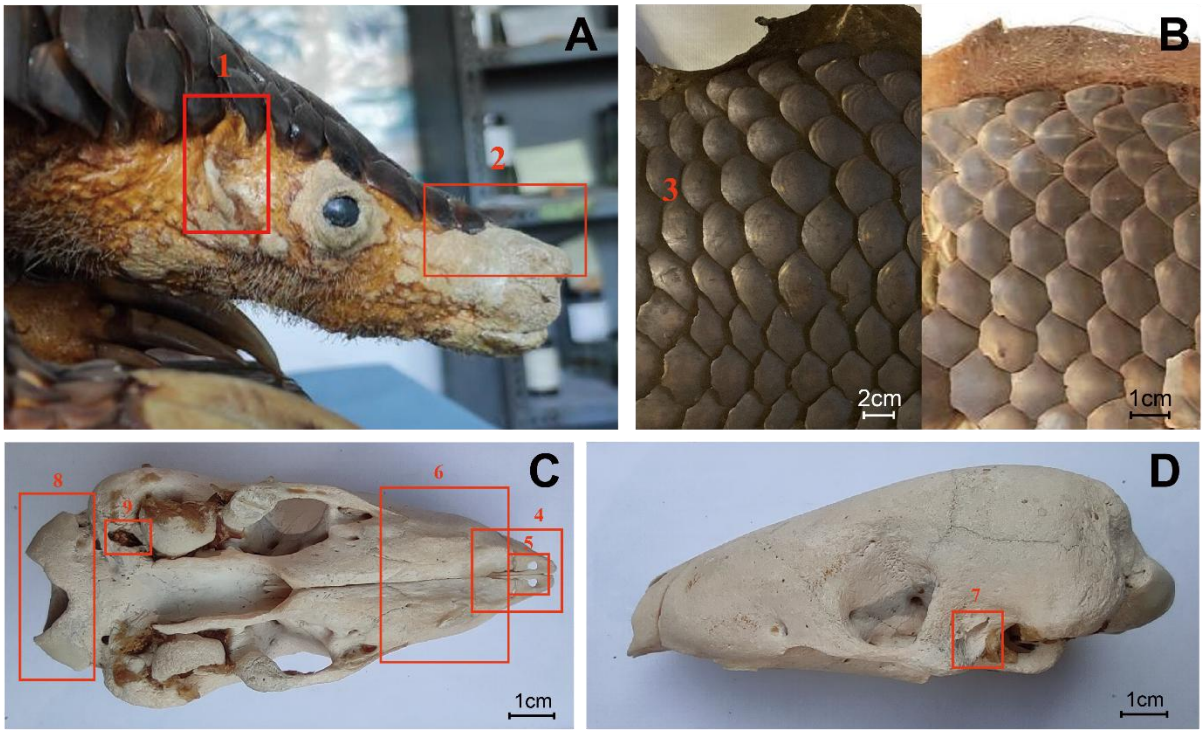

Fig S10. External morphology and skull characteristics of *M. aurita*. (A) Head of NHMTU-NP06. **(B)** Left: scale of BMNH 43.1.12.85; right: scale of NHMTU-NP07. **(C)** Ventral view of the skull of NHMTU-NP04. **(D)** Left lateral view of the skull of NHMTU-NP04. Numbers 1–9 indicate diagnostic features of *M. aurita*: 1. The external pinna is small and uniquely flake-shaped. 2. On the snout, the first row of head scales lies well behind the nasal tip, exposing a bare patch of naked skin. 3. Dorsal scales are smooth and trapezoidal with straight posterior margins, whereas the lateral scales near the abdomen are broad and shield-shaped. 4. The palatal process of the premaxilla extends posteriorly but measures less than half the premaxillary midline length. 5. The incisive foramen does not reach the premaxilla's posterior border. 6. At its anterior end, the maxilla bulges laterally, creating nearly parallel lateral margins. 7. In the middle of the postglenoid fossa, the postglenoid foramen opens laterally. 8. Both the jugular and hypoglossal foramina are recessed yet remain distinct. 9. The ventral surface of the occipital condyle is flat rather than convex.

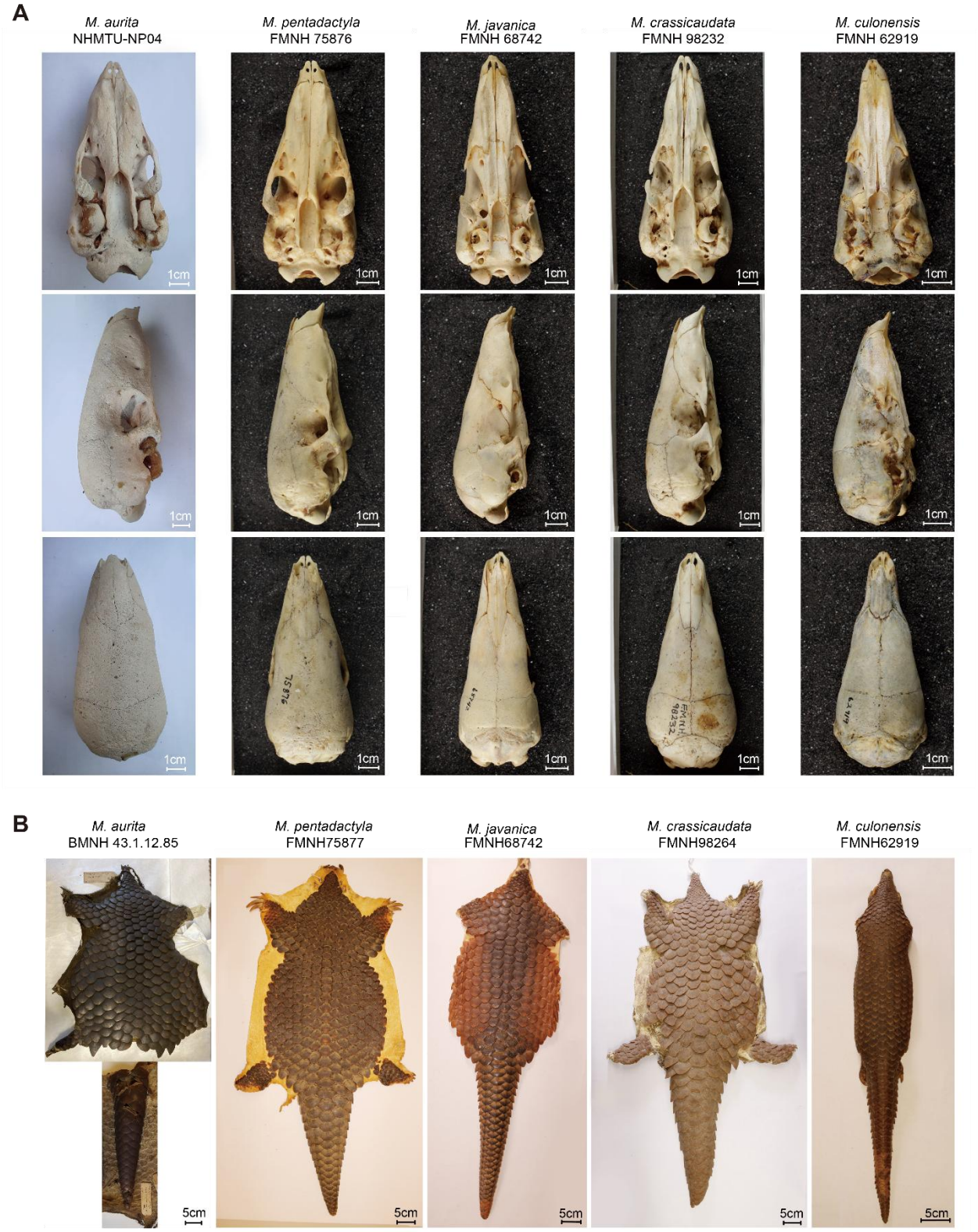

Fig S11. Skull and skin morphology of *Manis* species. (A) Ventral, lateral, and dorsal views of the pangolin skull. **(B)** Skin specimens of pangolins.

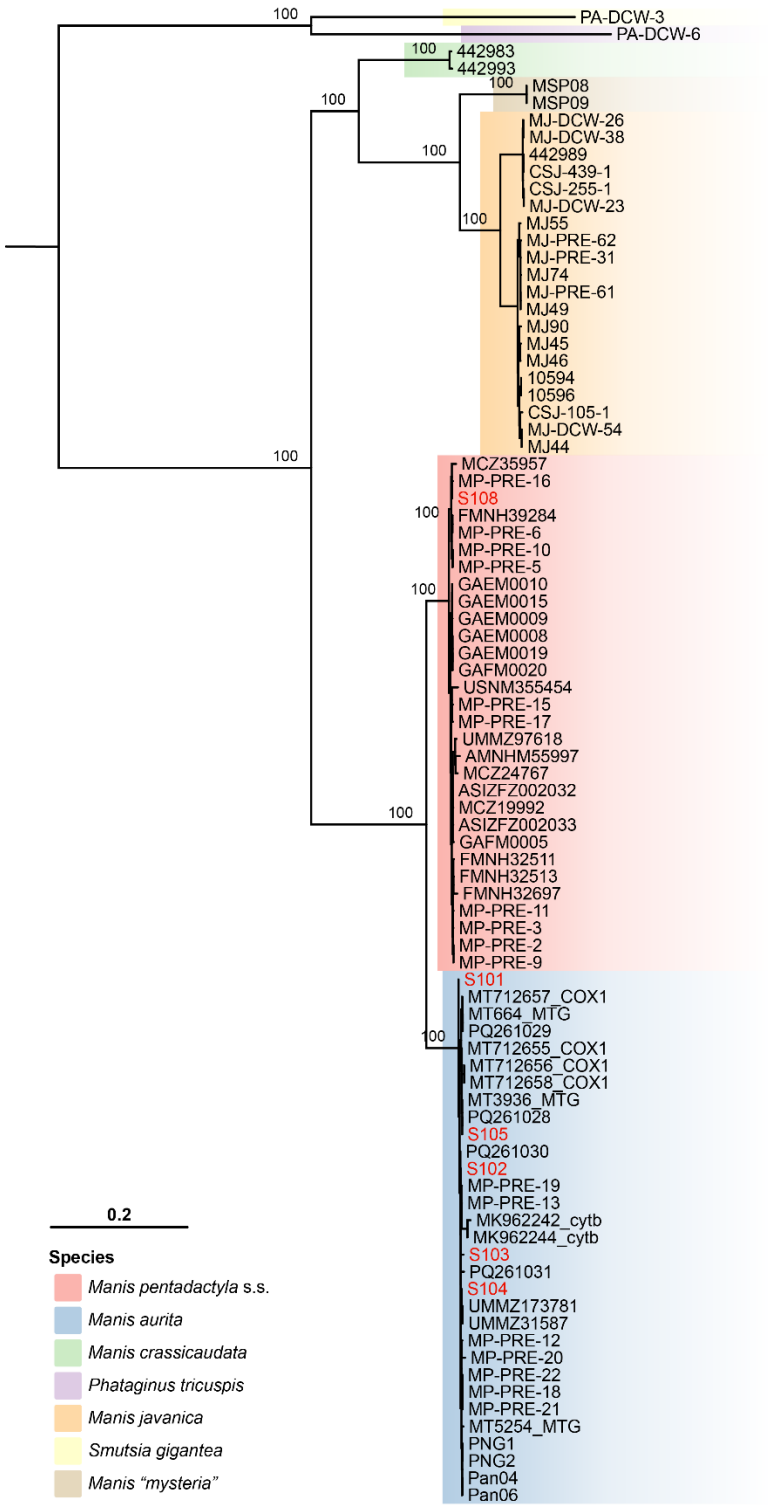

Fig. S12. Maximum Likelihood Phylogenetic Tree based on mitochondrial genomes, *CYTB and COI* using IQ-TREE with 1000 Bootstrap Replicates. Individuals highlighted in red were retrieved from Xie et al. (2021).